Table 1. Conventional echocardiographic parameters

	WT	*mdx*	*IL-10*$^{-/-}$	*IL-10*$^{-/-}$*/mdx*
HR (bpm)	185 ± 10	209 ± 9	189 ± 19	189 ± 19
EF (%)	79.4 ± 1.2	74.7 ± 3.7[a]	80.2 ± 0.1	65.6 ± 2.8[b]
FS (%)	42.0 ± 1.1	37.8 ± 3.2[a]	42.7 ± 0.9	30.9 ± 1.9[b]

Echocardiography was performed on 8–10-month-old mice. Comparisons of echocardiography values (mean ± SD) for wild-type (WT), *IL-10*$^{-/-}$, *mdx* and *IL-10*$^{-/-}$*/mdx* mice aged 8 months.
HR, heart rate; FS, fractional shortening; EF, ejection fraction.
[a]Difference ($P < 0.05$) between WT and *IL-10*$^{-/-}$ mice.
[b]Difference ($P < 0.01$) between WT, *IL-10*$^{-/-}$ and *mdx* mice.

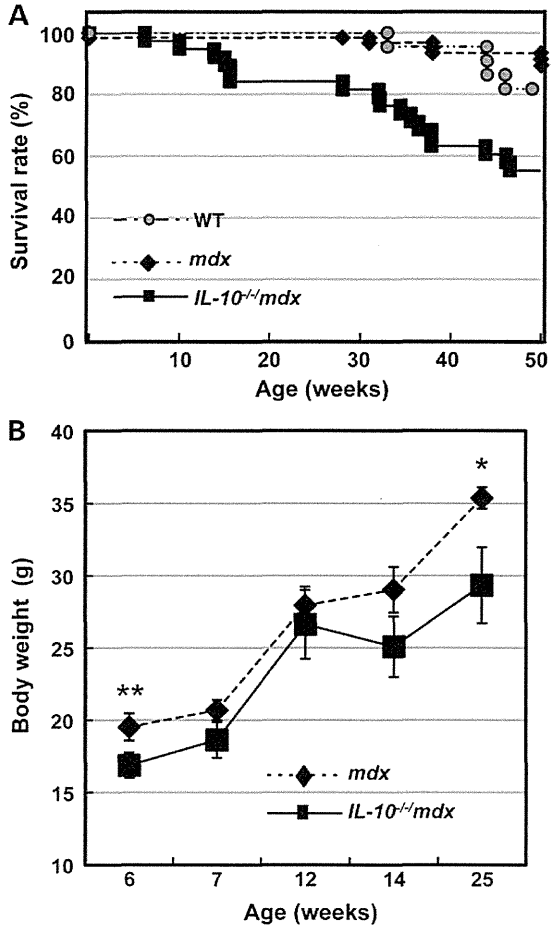

Figure 7. Reduced survival and early-life growth in *IL-10*$^{-/-}$*/mdx* mice. (**A**) Kaplan–Meier survival curves for wild-type, *mdx* and *IL-10*$^{-/-}$*/mdx* mice ($n = 7–37$, each). (**B**) Growth curves for WT, *mdx* and *IL-10*$^{-/-}$*/mdx* mice ($n = 4–6$, each group). Data are expressed as means ± SD. $^{*}P < 0.05$ and $^{**}P < 0.01$.

diaphragm and/or heart of aged *IL-10*$^{-/-}$*/mdx* mice. Nuclear factor κB (NF-κB) activity is thought to contribute the up-regulation of pro-inflammatory factors, because IL-10 inhibits NF-κB activation rather than several other transcriptional factors including NF-IL-6 and AP-1 (33). IL-16, a potent chemoattractant for several immune cells such as monocyte, and CD4^{+}T cells (34), would mediate further immune cell infiltration and activation in damaged muscle, similarly IL-1 and IL-1 receptor. Since IL-1β and IL-1ra are produced by M1 macrophages, our results suggest strong activation of M1 macrophages in IL-10-deficient dystrophic muscle. Whereas high level of TNF-α expression was known in the early phase of *mdx* mice (28), the TNF-α elevation in aged mice was not detectable in our immunoblot analysis (Fig. S2). However, up-regulation of TNF-α was confirmed in aged *IL-10*$^{-/-}$*/mdx* mice compared with *mdx* mice by ELISA analysis (Supplementary Material, Fig. S5). We also demonstrated that elevated TGF-β signaling and type-I collagen expression resulted in widespread fibrosis in the diaphragm and heart of *IL-10*$^{-/-}$*/mdx* mice lather than that of *mdx* mice (Figs 4 and 5). As previously reported, TGF-β is produced in response to fibrinogen stimulation of M1 macrophages via the intermediate induction of IL-1β (35). Since TGF-β was also reported to promote the TIMP-1 expression (36), up-regulated TIMP-1 may result in increased deposition of extracellular matrix through the TGF-β-TIMP-1 pathway and lead to tissue fibrosis. In the IL-10 regulated DMD muscle, active production of these inflammatory factors from infiltrating macrophages is associated with chronic inflammation to lead disease progression.

We demonstrated that the lack of IL-10 leads to respiratory dysfunction through severe inflammation and marked fibrosis in dystrophic diaphragm, without lung tissue damage (data not shown). The decreased tidal volume in *IL-10*$^{-/-}$*/mdx* mice (Fig. 6) might to be due to the apnea followed by hyperpnea (Supplementary Material, Fig. S4). Mice lacking both utrophin and dystrophin (*utrn*$^{-/-}$*/mdx*) exhibit a more severe DMD-like dystrophy with cardiomyopathy (37,38). *IL-10*$^{-/-}$*/mdx* mice exhibited similar respiratory dysfunction to *utrn*$^{-/-}$*/mdx* mice (data not shown), implying that respiratory dysfunction may be less dependent on membrane structure. *Utrn*$^{-/-}$*/mdx* mice died by 16–20 weeks due to severe DMD phenotypes (37,39), while 80% of *IL-10*$^{-/-}$*/mdx* mice were still alive at the same age (Fig. 7A). Furthermore, for breeding these mice, heterozygous for utrophin and either heterozygous for the dystrophin mutation (females) or hemizygous for the dystrophin mutation (males) are used to produce the *utrn*$^{-/-}$*/mdx* mice (37). On the other hand, IL-10-homozygous deficient *mdx* mice, homozygous females and hemizygous male mice, can be utilized to generate the littermates. In these contexts, *IL-10*$^{-/-}$*/mdx* mouse must be a quite useful model of DMD for long-term observation of disease phenotype under various therapeutic studies.

The most common manifestation of heart disease in DMD patient and *mdx* mice is dilated cardiomyopathy, which is characterized by a progressive decline in cardiac contractility, ventricular dilation and cardiac arrhythmias (40,41). A recent study showed that old IL-10 knockout mice develop left ventricle end-systolic diameter dilatation and heart enlargement with a reduction of EF% (42). Cardiac inflammation induced by IL-10 ablation induced cardiac dysfunction as the decreased LV function with LV and RV dilatation in *IL-10*$^{-/-}$*/mdx* mice (Table 1 and Fig. 4C).

In this study, we confirmed our hypothesis that a predisposition to inflammation causes chronic inflammation and results in more severe cardiorespiratory dysfunction by pathological

analysis using *IL-10*$^{-/-}$*/mdx* mice. Our findings are especially important for the development of effective therapies using anti-inflammatory drugs and/or immunomodulatory stem cells, such as mesenchymal stromal cells, to improve muscle and cardio-respiratory dysfunction.

MATERIALS AND METHODS

Animal care and sampling

All experimental procedures were approved by the Experimental Animal Care and Use Committee at the National Center of Neurology and Psychiatry (NCNP, Tokyo, Japan). C57BL/6-background *mdx* mice were a generous gift from Dr T. Sasaoka (National Institute for Basic Biology, Aichi, Japan) and were maintained in our animal facility. C57BL/6J (WT) mice were purchased from Nihon CLEA (Tokyo, Japan). Mice carrying null mutation for IL-10 that had been back-crossed onto a C57/BL6 background, B10.129P2(B6)-*Il10*^{tm1Cgn}/J mice, were purchased from The Jackson Laboratory (Bar Harbor, ME, USA). IL-10 knockout (B10.129P2(B6)-*Il10*^{tm1Cgn}/J) mice were crossed with *mdx* mice to generate mice that lacked both IL-10 and dystrophin. All animals were maintained according to the standard protocol for animal care at the NCNP. Genotyping to detect the mutated alleles of IL-10 and dystrophin was performed by PCR. Null mutation of the dystrophin gene was confirmed using *mdx*-amplification-resistant mutation system PCR (43). Age-matched littermate mice (3-, 8-, and12-month-old) were used for experiments. Samples from heart, diaphragm and TA muscle were taken and immediately frozen in liquid nitrogen-cooled isopentane. Six to eight mice from each group were used for analysis at each time point.

Histopathology and immunohistochemistry

Transverse cryosections (10 μm thick) prepared from heart, diaphragm and TA muscle were stained with hematoxylin and eosin (H&E) using standard procedures. For immunohistochemistry, 8 μm thick cryosections were fixed in 1% paraformaldehyde–PBS for 30 min at 4°C, treated with Triton X-100 and then blocked with 3% bovine serum albumin (BSA) in PBS. The following antibodies were used at 1:50–1:100 dilutions for macrophage detection: rabbit anti-mouse CD68 antibodies (Abcam, Cambridge, UK), rat anti-mouse CD206 antibodies (Bio-Rad Laboratories, Inc., Hercules, CA, USA). All antibodies were diluted with PBS containing 0.5% BSA and incubated with the tissue sections for either 1 h at room temperature or overnight at 4°C. The tissue sections were washed with PBS and then incubated with Alexa 488- or Alexa 594-conjugated anti-rabbit or rat IgG antibodies (Life Technologies, Carlsbad, CA, USA), at 1:500 dilution for 1 h at 4°C according to the MOM procedure (Vector Laboratories, Burlingame, CA, USA). Glass slides were washed with PBS and mounted in Vectashield (Vector Laboratories) with 4′,6′-diamidino-2-phenylind ole (DAPI). Immunofluorescence was visualized using an IX71 fluorescence microscope (Olympus, Tokyo, Japan) and BZ-X700, BZ-9000 (KEYENCE, Osaka, Japan). For estimation of fibrosis, sections taken from frozen heart and diaphragm samples were stained in sirius-red solution or Masson's trichrome solution, as previously described (44).

Proteome profiler cytokine array

Muscle tissue samples were disrupted in a Multi-Beads Shocker (Yasui Kikai, Osaka, Japan) and the protein concentrations were determined using the Pierce® BCA Protein Assay Kit (Thermo Fisher Scientific Inc., IL, USA). The relative expression of cytokines and chemokines in muscle lysates was quantified using the Proteome Profiler™ Array (Mouse Cytokine Array, Panel A; R&D Systems Inc., Minneapolis, MN, USA). The array was performed according to the manufacturer's exact specifications using 250 μl plasma ($n = 8$). To achieve maximum assay sensitivity, the blots were incubated with plasma for overnight. ECL incubation was performed for 5 min using the Super Signal West Femto Chemiluminescent Kit (Thermo Scientific Pierce, Rockford, IL, USA), and then images were captured and analyzed using Image Quant LAS 4000 coupled with Image Quant TL software (GE Healthcare).

ELISA

The amount of TGF-β1 and type I collagen in muscle lysate obtained from diaphragm and heart was determined by the Quantikine ELISA mouse TGF-β1 immunoassay (R&D Systems, Inc.) and the mouse collagen type 1 (Col1) ELISA kit (Cloud-Clone Corp., TX, USA) according to the manufacturer's recommendations. Final values were normalized for protein concentration.

Assessment of respiratory function

Mouse respiratory function was evaluated by whole-body plethysmography. The plethysmograph was composed of two Plexiglas cylinders, one serving as the animal chamber and the other as reference chamber, and each unrestrained conscious 3- and 8-month-old mouse was placed in a 'free moving' chamber. RR and TV were assessed by a respiration monitoring system (Model RM-80, Columbus Instruments, Columbus, OH, USA). The signal was digitized using a Power Lab data acquisition system with Chart-Pro 6 software (AD Instruments, Dunedin, New Zealand) for recording and analysis.

Echocardiography

Mice were anesthetized by 2% isoflurane inhalation (Univentor 400 Anaesthesia unit, Univentor Limited, Malta). After shaving their chest, the mice were imaged using Vivid-i Dimensions (GE Vingmed, Horten, Norway) equipped with a transducer (i12-RS) transmitting at 10 MHz echocardiographic probe. Standard gray scale M- and B-mode images were acquired using a parasternal long- and short-axis view. For the basic measurements of left ventricular function, %FS and EF% were examined using M-mode echocardiography.

SUPPLEMENTARY MATERIAL

Supplementary Material is available at *HMG* online.

ACKNOWLEDGMENTS

The authors thank Akinori Nakamura, Tetsuya Nagata, Jun Tanihata, Kazumi Motoki, Michihiro Imamura, Naoki Itoh, Kazuhiro Yamamoto, Masayuki Sekiguchi, Hiroshi Takano and Yoko Fujii for technical advice, support and helpful discussions; Ryoko Nakagawa, Shota Saka and Nana Tsumita for technical assistance. We also thank for the research support from JCR Pharmaceuticals Co., Ltd.

Conflict of Interest statement. We received the research support from JCR Pharmaceuticals Co., Ltd. and TaKaRa Bio Inc.

FUNDING

This work was supported by the research grant from JCR Pharmaceuticals Co., Ltd., Health Sciences Research Grants for Research on Human Genome and Gene Therapy from the Ministry of Health, Labor and Welfare of Japan (grant number: 21A-3), and a Grant-in-Aid for Scientific Research from the Ministry of Education, Culture, Sports, Science and Technology (grant number: 22390284, 22-40134).

REFERENCES

1. Moser, H. (1984) Duchenne muscular dystrophy: pathogenetic aspects and genetic prevention. *Hum. Genet.*, **66**, 17–40.
2. Koenig, M., Hoffman, E.P., Bertelson, C.J., Monaco, A.P., Feener, C. and Kunkel, L.M. (1987) Complete cloning of the Duchenne muscular dystrophy (DMD) cDNA and preliminary genomic organization of the DMD gene in normal and affected individuals. *Cell*, **50**, 509–517.
3. Ervasti, J.M., Ohlendieck, K., Kahl, S.D., Gaver, M.G. and Campbell, K.P. (1990) Deficiency of a glycoprotein component of the dystrophin complex in dystrophic muscle. *Nature*, **345**, 315–319.
4. Hahn, A., Bach, J.R., Delaubier, A., Renardel-Irani, A., Guillou, C. and Rideau, Y. (1997) Clinical implications of maximal respiratory pressure determinations for individuals with Duchenne muscular dystrophy. *Arch. Phys. Med. Rehabil.*, **78**, 1–6.
5. Manzur, A.Y., Kuntzer, T., Pike, M. and Swan, A. (2008) Glucocorticoid corticosteroids for Duchenne muscular dystrophy. *Cochrane Database Syst. Rev.*, **1**, CD003725.
6. Mantovani, A., Sica, A., Sozzani, S., Allavena, P., Vecchi, A. and Locati, M. (2004) The chemokine system in diverse forms of macrophage activation and polarization. *Trends Immunol.*, **25**, 677–686.
7. Moxley, R.T. 3rd, Ashwal, S., Pandya, S., Connolly, A., Florence, J., Mathews, K., Baumbach, L., McDonald, C., Sussman, M. and Wade, C. (2005) Practice parameter: corticosteroid treatment of Duchenne dystrophy: report of the Quality Standards Subcommittee of the American Academy of Neurology and the Practice Committee of the Child Neurology Society. *Neurology*, **64**, 13–20.
8. Spencer, M.J., Montecino-Rodriguez, E., Dorshkind, K. and Tidball, J.G. (2001) Helper (CD4(+)) and cytotoxic (CD8(+)) T cells promote the pathology of dystrophin-deficient muscle. *Clin. Immunol.*, **98**, 235–243.
9. Arahata, K. and Engel, A.G. (1984) Monoclonal antibody analysis of mononuclear cells in myopathies. I: quantitation of subsets according to diagnosis and sites of accumulation and demonstration and counts of muscle fibers invaded by T cells. *Ann. Neurol.*, **16**, 193–208.
10. Engel, A.G. and Arahata, K. (1986) Mononuclear cells in myopathies: quantitation of functionally distinct subsets, recognition of antigen-specific cell-mediated cytotoxicity in some diseases, and implications for the pathogenesis of the different inflammatory myopathies. *Hum. Pathol.*, **17**, 704–721.
11. Cai, B., Spencer, M.J., Nakamura, G., Tseng-Ong, L. and Tidball, J.G. (2000) Eosinophilia of dystrophin-deficient muscle is promoted by perforin-mediated cytotoxicity by T cell effectors. *Am. J. Pathol.*, **156**, 1789–1796.
12. Gorospe, J.R., Tharp, M., Demitsu, T. and Hoffman, E.P. (1994) Dystrophin-deficient myofibers are vulnerable to mast cell granule-induced necrosis. *Neuromuscul. Disord.*, **4**, 325–333.
13. Hussein, M.R., Hamed, S.A., Mostafa, M.G., Abu-Dief, E.E., Kamel, N.F. and Kandil, M.R. (2006) The effects of glucocorticoid therapy on the inflammatory and dendritic cells in muscular dystrophies. *Int. J. Exp. Pathol.*, **87**, 451–461.
14. Hodgetts, S., Radley, H., Davies, M. and Grounds, M.D. (2006) Reduced necrosis of dystrophic muscle by depletion of host neutrophils, or blocking TNFalpha function with Etanercept in mdx mice. *Neuromuscul. Disord.*, **16**, 591–602.
15. Radley, H.G. and Grounds, M.D. (2006) Cromolyn administration (to block mast cell degranulation) reduces necrosis of dystrophic muscle in mdx mice. *Neurobiol. Dis.*, **23**, 387–397.
16. Pasternak, C., Wong, S. and Elson, E.L. (1995) Mechanical function of dystrophin in muscle cells. *J. Cell Biol.*, **128**, 355–361.
17. Petrof, B.J., Shrager, J.B., Stedman, H.H., Kelly, A.M. and Sweeney, H.L. (1993) Dystrophin protects the sarcolemma from stresses developed during muscle contraction. *Proc. Natl Acad. Sci. USA*, **90**, 3710–3714.
18. Bulfield, G., Siller, W.G., Wight, P.A. and Moore, K.J. (1984) X chromosome-linked muscular dystrophy (mdx) in the mouse. *Proc. Natl Acad. Sci. USA*, **81**, 1189–1192.
19. Villalta, S.A., Nguyen, H.X., Deng, B., Gotoh, T. and Tidball, J.G. (2009) Shifts in macrophage phenotypes and macrophage competition for arginine metabolism affect the severity of muscle pathology in muscular dystrophy. *Hum. Mol. Genet.*, **18**, 482–496.
20. Villalta, S.A., Rinaldi, C., Deng, B., Liu, G., Fedor, B. and Tidball, J.G. (2011) Interleukin-10 reduces the pathology of mdx muscular dystrophy by deactivating M1 macrophages and modulating macrophage phenotype. *Hum. Mol. Genet.*, **20**, 790–805.
21. Tso, V.K., Sydora, B.C., Foshaug, R.R., Churchill, T.A., Doyle, J., Slupsky, C.M. and Fedorak, R.N. (2013) Metabolomic profiles are gender, disease and time specific in the interleukin-10 gene-deficient mouse model of inflammatory bowel disease. *PLoS ONE*, **8**, e67654.
22. Yang, I., Eibach, D., Kops, F., Brenneke, B., Woltemate, S., Schulze, J., Bleich, A., Gruber, A.D., Muthupalani, S., Fox, J.G. *et al.* (2013) Intestinal microbiota composition of interleukin-10 deficient C57BL/6J mice and susceptibility to helicobacter hepaticus-induced colitis. *PLoS ONE*, **8**, e70783.
23. Tidball, J.G. (1995) Inflammatory cell response to acute muscle injury. *Med. Sci. Sports Exerc.*, **27**, 1022–1032.
24. Hosaka, Y., Yokota, T., Miyagoe-Suzuki, Y., Yuasa, K., Imamura, M., Matsuda, R., Ikemoto, T., Kameya, S. and Takeda, S. (2002) Alpha1-syntrophin-deficient skeletal muscle exhibits hypertrophy and aberrant formation of neuromuscular junctions during regeneration. *J. Cell Biol.*, **158**, 1097–1107.
25. Tidball, J.G. and Villalta, S.A. (2010) Regulatory interactions between muscle and the immune system during muscle regeneration. *Am. J. Physiol. Regul. Integr. Comp. Physiol.*, **298**, R1173–R1187.
26. Pastoret, C. and Sebille, A. (1995) Age-related differences in regeneration of dystrophic (mdx) and normal muscle in the mouse. *Muscle Nerve*, **18**, 1147–1154.
27. Anderson, J.E., McIntosh, L.M. and Poettcker, R. (1996) Deflazacort but not prednisone improves both muscle repair and fiber growth in diaphragm and limb muscle in vivo in the mdx dystrophic mouse. *Muscle Nerve*, **19**, 1576–1585.
28. Evans, N.P., Misyak, S.A., Robertson, J.L., Bassaganya-Riera, J. and Grange, R.W. (2009) Immune-mediated mechanisms potentially regulate the disease time-course of duchenne muscular dystrophy and provide targets for therapeutic intervention. *PMR*, **1**, 755–768.
29. Wehling, M., Spencer, M.J. and Tidball, J.G. (2001) A nitric oxide synthase transgene ameliorates muscular dystrophy in mdx mice. *J. Cell Biol.*, **155**, 123–131.
30. Spencer, M.J., Marino, M.W. and Winckler, W.M. (2000) Altered pathological progression of diaphragm and quadriceps muscle in TNF-deficient, dystrophin-deficient mice. *Neuromuscul. Disord.*, **10**, 612–619.
31. Pescatori, M., Broccolini, A., Minetti, C., Bertini, E., Bruno, C., D'Amico, A., Bernardini, C., Mirabella, M., Silvestri, G., Giglio, V. *et al.* (2007) Gene expression profiling in the early phases of DMD: a constant molecular signature characterizes DMD muscle from early postnatal life throughout disease progression. *FASEB J.*, **21**, 1210–1226.

32. Villalta, S.A., Deng, B., Rinaldi, C., Wehling-Henricks, M. and Tidball, J.G. (2011) IFN-gamma promotes muscle damage in the mdx mouse model of Duchenne muscular dystrophy by suppressing M2 macrophage activation and inhibiting muscle cell proliferation. *J. Immunol.*, **187**, 5419–5428.
33. Wang, P., Wu, P., Siegel, M.I., Egan, R.W. and Billah, M.M. (1995) Interleukin (IL)-10 inhibits nuclear factor kappa B (NF kappa B) activation in human monocytes. IL-10 and IL-4 suppress cytokine synthesis by different mechanisms. *J. Biol. Chem.*, **270**, 9558–9563.
34. Cruikshank, W.W., Kornfeld, H. and Center, D.M. (2000) Interleukin-16. *J. Leukoc. Biol.*, **67**, 757–766.
35. Vidal, B., Serrano, A.L., Tjwa, M., Suelves, M., Ardite, E., De Mori, R., Baeza-Raja, B., Martinez de Lagran, M., Lafuste, P., Ruiz-Bonilla, V. *et al.* (2008) Fibrinogen drives dystrophic muscle fibrosis via a TGFbeta/alternative macrophage activation pathway. *Genes Dev.*, **22**, 1747–1752.
36. Eickelberg, O., Kohler, E., Reichenberger, F., Bertschin, S., Woodtli, T., Erne, P., Perruchoud, A.P. and Roth, M. (1999) Extracellular matrix deposition by primary human lung fibroblasts in response to TGF-beta1 and TGF-beta3. *Am. J. Physiol.*, **276**, L814–L824.
37. Deconinck, A.E., Rafael, J.A., Skinner, J.A., Brown, S.C., Potter, A.C., Metzinger, L., Watt, D.J., Dickson, J.G., Tinsley, J.M. and Davies, K.E. (1997) Utrophin-dystrophin-deficient mice as a model for Duchenne muscular dystrophy. *Cell*, **90**, 717–727.
38. Grady, R.M., Teng, H., Nichol, M.C., Cunningham, J.C., Wilkinson, R.S. and Sanes, J.R. (1997) Skeletal and cardiac myopathies in mice lacking utrophin and dystrophin: a model for Duchenne muscular dystrophy. *Cell*, **90**, 729–738.
39. Wang, B., Li, J., Fu, F.H. and Xiao, X. (2009) Systemic human minidystrophin gene transfer improves functions and life span of dystrophin and dystrophin/utrophin-deficient mice. *J. Orthop. Res.*, **27**, 421–426.
40. Ferlini, A., Sewry, C., Melis, M.A., Mateddu, A. and Muntoni, F. (1999) X-linked dilated cardiomyopathy and the dystrophin gene. *Neuromuscul. Disord.*, **9**, 339–346.
41. Buyse, G.M., Van der Mieren, G., Erb, M., D'Hooge, J., Herijgers, P., Verbeken, E., Jara, A., Van Den Bergh, A., Mertens, L., Courdier-Fruh, I. *et al.* (2009) Long-term blinded placebo-controlled study of SNT-MC17/idebenone in the dystrophin deficient mdx mouse: cardiac protection and improved exercise performance. *Eur. Heart J.*, **30**, 116–124.
42. Sikka, G., Miller, K.L., Steppan, J., Pandey, D., Jung, S.M., Fraser, C.D. 3rd, Ellis, C., Ross, D., Vandegaer, K., Bedja, D. *et al.* (2013) Interleukin 10 knockout frail mice develop cardiac and vascular dysfunction with increased age. *Exp. Gerontol.*, **48**, 128–135.
43. Amalfitano, A. and Chamberlain, J.S. (1996) The mdx-amplification-resistant mutation system assay, a simple and rapid polymerase chain reaction-based detection of the mdx allele. *Muscle Nerve*, **19**, 1549–1553.
44. Shin, J.H., Nitahara-Kasahara, Y., Hayashita-Kinoh, H., Ohshima-Hosoyama, S., Kinoshita, K., Chiyo, T., Okada, H., Okada, T. and Takeda, S. (2011) Improvement of cardiac fibrosis in dystrophic mice by rAAV9-mediated microdystrophin transduction. *Gene Ther.*, **18**, 910–919.

Mini Review

Cell therapeutic approaches using multipotent mesenchymal stromal cells for muscular dystrophy

Yuko Nitahara-Kasahara[1)], Shin'ichi Takeda[1)] and Takashi Okada[1, 2, *)]

[1)]Department of Molecular Therapy, National Institute of Neuroscience, National Center of Neurology and Psychiatry, Tokyo, Japan

[2)]Department of Biochemistry and Molecular Biology, Division of Gene Therapy Research, Center for Advanced Medical Technology, Nippon Medical School, Tokyo, Japan

Multipotent mesenchymal stromal cells (MSCs) have potential therapeutic uses owing to their ability to differentiate *in situ* into various cell types with immunosuppressive properties. Clinically, MSCs have been used to treat inflammatory diseases, such as steroid-resistant graft-versus-host disease. We previously reported a strategy to expand MSC cultures and to induce these cells to undergo myogenic differentiation, which is promising for the treatment of muscular diseases. Muscular dystrophy is an incurable genetic disease with early mortality and causes skeletal muscle weakness with chronic inflammation. Here, we focused on the beneficial properties of MSCs, namely, they can undergo mesoderm differentiation, have the ability to fuse with dystrophic muscles, and have anti-inflammatory activities. In this review, we highlight and discuss MSC-based therapeutic approaches for muscular dystrophy.

Rec.1/22/2014, Acc.9/12/2014, pp198-205

*Correspondence should be addressed to:
Takashi Okada, Department of Biochemistry and Molecular Biology, Division of Gene Therapy Research, Center for Advanced Medical Technology, Nippon Medical School, 1-1-5 Sendagi, Bunkyo-ku, Tokyo 113-8602, Japan. Phone: +81-3-3822-2131, Fax: +81-3-5814-8156, E-mail: t-okada@nms.ac.jp

Key words multipotent mesenchymal stromal cells, anti-inflammation, muscular dystrophy, muscular differentiation, cell transplantation

Introduction

Multipotent mesenchymal stromal cells (MSCs) from bone-marrow are conventionally defined as adherent non-hematopoietic cells that express several cell surface antigenic markers, such as CD44, CD73, CD90, and CD105, but not the hematopoietic markers CD34 or CD45[1)]. Although they were originally identified in bone-marrow[1)], MSCs can be extracted from numerous tissues including

adipose tissue[2], heart tissue[3], Wharton's jelly[4], dental pulp[5], peripheral blood[6], cord blood[7], menstrual blood[8-10], and fallopian tube tissue[11]. MSCs have been extensively studied owing to their ability to self-renew and differentiate into many different cell types in culture, particularly cells of mesodermal origin such as osteoblasts, chondrocytes, adipocytes, and myocytes[12, 13]. Furthermore, MSCs can also differentiate into cells of non-mesodermal origin, such as hepatocytes[14, 15], neural cells[16], and epithelial cells[17]. MSCs can influence immune effector cell development, maturation, and function, as well as alloreactive T-cell responses, through the production of bioactive cytokines and proteins[18]. The multilineage potential of MSCs has been further exploited in their potential use as therapies for various diseases, which is feasible because these cells can be readily obtained from patients, are easily expanded in culture, and are not tumorigenic. Furthermore, the use of third-party MSCs in cell therapies is facilitated by the fact that these cells are immunoprivileged because they do not express human leukocyte antigen (HLA) class II proteins, CD40, CD80, or CD86[19], and express only low levels of HLA class I proteins. Consequently, MSCs are not lysed by natural killer (NK) cells or cytotoxic T lymphocytes[20].

Recently, MSCs have obtained market authorization as a product for the treatment of acute graft-versus-host disease (GVHD) in Canada and New Zealand. MSCs are being evaluated in Phase 3 clinical trials to treat Crohn's disease and acute radiation syndrome, and in Phase 2 trials to treat several ailments such as type I diabetes, acute myocardial infraction, and pulmonary disease (Mesoblast Inc., http://www.mesoblast.com/products/overview). Furthermore, MSCs are extremely attractive candidates for cell-based strategies that target other diseases such as muscular disease[21]. In this review, we discuss how MSC therapy might have beneficial effects on the progression of muscular dystrophy via eliciting anti-inflammatory effects and/or promoting the regeneration of myofibers.

Myogenic differentiation of MSCs

MSCs themselves can be induced to differentiate along the myogenic pathway, thereby fusing with myotubes and promoting the formation of new muscle fibers after being transplanted into muscle tissue[22].

MSCs can form muscle cells after treatment with one or a combination of 5'-azacytidine (a demethylating agent), hydrocortisone[23], dexamethasone, ascorbic acid, and growth factors, when co-cultured with immortalized myoblast cells (C2C12)[24, 25], or when exposed to the conditioned media of these cells[26]. A method has been reported to induce skeletal muscle lineage cells from human and rat adherent MSCs via transduction with the Notch1 intracellular domain and administration of certain trophic factors and cytokines[22]. Upon genetic modification with a lentiviral vector encoding Pax3, which is the master regulator of the embryonic myogenic program, expression of myogenic regulatory factors is activated in human MSCs after 4 weeks of culture, suggesting that Pax3 enables MSCs to differentiate into myogenic progenitors *in vitro*[27].

We have also reported efficient methods to expand MSC cultures obtained from dog bone-marrow and to induce the myogenic differentiation of these cells[21]. CD271 is a marker of progenitor cells and bone-marrow-derived MSCs[28]. MSC cultures enriched in $CD271^+$ cells grow better than CD271-depleted cultures. Transduction of $CD271^+$ MSCs with MyoD-expressing adenovirus vector, as an inducer of myogenic differentiation, causes the formation of myotubes that express late myogenic markers. These methods may be useful to efficiently transplant cells for the treatment of muscle disease.

Paracrine effects of MSCs

MSCs secrete distinctively different cytokines and chemokines, such as greater amounts of VEGF-α, IGF-1, EGF, keratinocyte growth factor, angiopoietin-1, stromal derived factor-1, macrophage inflammatory protein-1α and β and erythropoietin[29], After transplantation, MSCs home to interstitial muscle tissue and localize close to satellite cells. MSCs induce the myogenic differentiation of neighboring satellite cells, as evidenced by the finding that isolated cells from muscle in which MSCs have engrafted show high myogenic activity and displayed $CD45^-$, $sca\text{-}1^-$, $Mac\text{-}1^-$, $CD34^+$, $CXCR4^+$, $\beta1\text{-integrin}^+$ characteristics[30]. Clinical interest in the application of MSCs in cell therapies is not only owing to their ability to differentiate, but also to their release of cytokines into the surrounding environment, which modifies the developmental fate of neighboring cells in a paracrine manner.

Cell therapeutic approach for muscular dystrophy

In this section, we discuss whether the myogenic differentiation of MSCs beneficially affects the progression of muscular dystrophy. Muscular dystrophy patients exhibit skeletal muscle damage that is associated with chronic

inflammation, numerous centrally nucleated fibers, and continuous cycles of myofiber degeneration/necrosis and regeneration. In particular, Duchenne muscular dystrophy (DMD) is a severe X-linked muscle disease in which mutations in the gene encoding the cytoskeletal protein dystrophin result in destruction of the dystrophin-glycoprotein complexes of the sarcolemma[31, 32]. The resulting alterations in mechanical and signaling functions contribute to membrane fragility, necrosis, and immune cell infiltration, and cause progressive degeneration of striated muscle. The pathology of DMD muscles leads to chronic inflammation, fibrosis, fat infiltration, and impaired vasoregulation, manifesting as muscle weakness and eventually skeletal muscle atrophy[33, 34]. As the disease progresses, wheelchairs and ventilatory assistance are required, and patients often succumb to cardiac dysfunction and respiratory failure[35].

Cell-based therapies for DMD have the potential to restore dystrophin expression and, therefore, also the parenchyma of muscle. The following section introduces the general concepts behind gene- and cell-based strategies to treat DMD. Transplantation of mesoangioblasts, hematopoietic stem cells, myoblasts, and muscle-derived stem cells has been examined as a possible strategy to treat DMD and as a system to deliver therapeutic recombinant proteins to target muscle tissues[36-38].

In dystrophin-deficient *mdx* mice, transplanted human MSCs were incorporated into myofibers and dystrophin expression was subsequently restored[22, 39, 40]. MSCs transduced with Notch1 and treated with trophic factors and cytokines can differentiate when transplanted into the degenerated muscles of rats and *mdx*-nude mice. The induced population contains Pax7$^+$ cells that contribute to the subsequent regeneration of muscles[22]. Transplantation of human adipose-derived MSCs transduced with a MyoD-coding lentiviral vector into the injured muscles of immunodepressed Rag2$^{-/-}\gamma C^{-/-}$ mice resulted in a substantial increase in the number of myofibers and restoration of dystrophic expression[41]. Although the engraftment of human MSCs from bone-marrow is improved in the presence of Pax3, supported by an approximately 1.3-fold increase in the level of myofibers in immunodepressed mdx mice, this engraftment is not accompanied by functional recovery[27].

In therapeutic approaches using medium-sized animal models of DMD, such as dogs, transplantation of heterologous mesoangioblasts in golden retriever muscular dystrophy (GRMD) ameliorated and preserved active motility[42]. However, the development of an analogous approach for clinical use in humans has been hindered by the inability to overcome several obstacles, including poor cell survival rates, limited dissemination of injected cells, immune responses to allogeneic cells, the presence of the neotransgene product in dystrophic muscles, and the inability to specifically target the cells to particular regions, such as cardiac tissue[43].

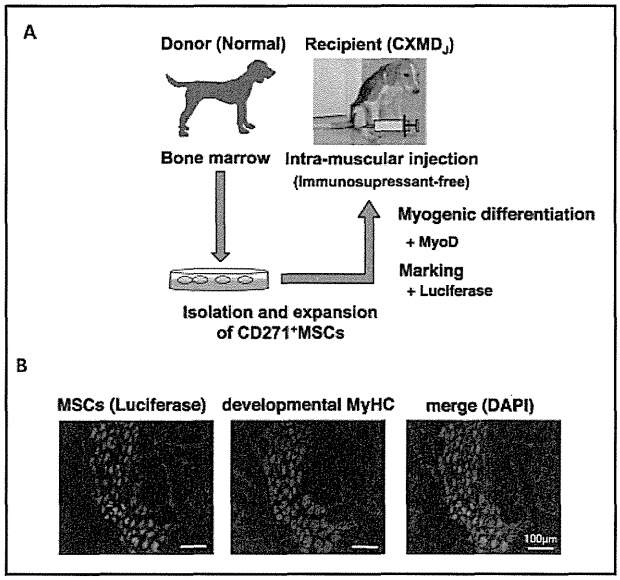

Fig.1 Successful long-term engraftment and myogenic differentiation of CD271$^+$ MSCs

(A) Transplantation procedure. CD271$^+$ mesenchymal stem cells (MSCs) were enriched from the bone-marrow of healthy dogs and expanded. These cells were transduced with a luciferase-expressing lentivirus vector as a marker and a MyoD-expressing adenoviral vector, and injected into Duchenne muscular dystrophy dogs without immunosuppressants. (B) Engraftment and differentiation. At 12 weeks after CD271$^+$ MSCs injection, cryosections from the muscle of recipients were stained with antibodies specific for luciferase expressed in MSCs (green) and the myogenic marker developmental myosin heavy chain (dMyHC) (red). The merged image includes staining of nuclei with 4', 6'-diamidino-2-phenylindole (DAPI) (blue). CD271$^+$ MSCs formed muscle-like tissue that expressed dMyHC at 12 weeks after transplantation (Quote from ref. 21) with minor revision).

In our previous study, we found that wild-type CD271$^+$ MSCs in a myogenic cell lineage transplanted into dogs with X-linked muscular dystrophy in Japan (CXMDJ) formed clusters of muscle-like tissues within 8-12 weeks in the absence of immunosuppression[21] (Fig.1). In the newly formed tissues, expression of developmental myosin heavy chain, which is a marker of myogenesis, and dystrophin

was up-regulated. In CXMD$_J$, transplanted MSCs that are delivered systemically must specifically engraft into muscle tissue. MSCs normally mobilize in the blood in response to skeletal muscle injury[44], and several homing/migration/engraftment studies have suggested that MSCs delivered systemically can "home" to the site of injury[45-49]. Intra-arterial injection of CD271$^+$ MSCs results in engraftment at the site of acutely injured muscle and the formation of muscle fibers[21]. These findings suggest that a cell transplantation strategy using CD271$^+$ MSCs is a promising treatment approach for DMD.

Human immature dental pulp stem cells (hIDPSCs), which are obtained from decidual tooth tissue and comprise a homogeneous population positive for MSC markers, are a more convenient cell source than bone-marrow. These cells are similar to populations of dental pulp MSCs with immunosuppressive activity[50]. The proliferation and neurogenicity of hIDPSCs in dental pulp are more potent than those of bone-marrow MSCs, probably because the former cells are of neural crest origin. hIDPSCs inhibit the proliferation of phytohemagglutinin-stimulated T-cells, and therefore would elicit stronger effects than bone-marrow MSCs[50, 51]. After transplantation of hIDPSCs into young GRMD dogs without immunosuppression, a limited number of muscle fibers express dystrophin[52].

These approaches using MSCs need to be further developed to obtain fully differentiated muscle fibers and to stimulate functional recovery of skeletal muscles in DMD patients.

Therapeutic approach using the immunomodulatory properties of MSCs

MSCs regulate inflammation through mechanisms thought to involve the inhibition of monocyte differentiation into immature dendritic cells (DCs)[53]. This results in the skewing of DCs toward macrophages[54, 55], suppression of DC maturation[54, 56], inhibition of T-cell and B-cell proliferation, suppression of NK and cytotoxic T cell function[57], and inhibition of neutrophil apoptosis, inducing the generation of regulatory T-cells[58] (Fig.2). Therefore, the effects of MSCs on immune diseases have been investigated[59, 60]. Furthermore, interleukin (IL)-10-transfected MSCs can reduce the severity of acute GVHD and aid the recovery of cardiac function due to high levels of immunosuppression[61, 62]. Another study reported that human amniotic membrane-derived mesenchymal cells (hAMCs) markedly increase HLA-G expression *in vitro* following administration of IL-10

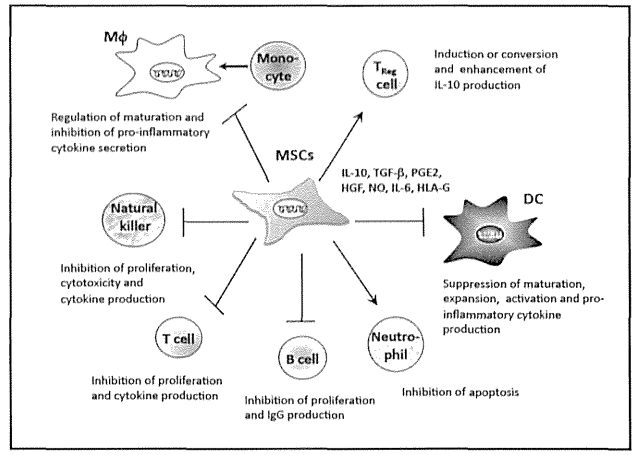

Fig.2 Immunoregulation by mesenchymal stems cells (MSCs)
The immunoregulation of various cell types by MSCs through IL-10, TGF-β, PGE2, HGF, NO, and HLA-G is shown.

or progesterone, which plays an important role in feto-maternal tolerance during pregnancy, and, surprisingly, also increases the efficiency of cardiomyogenic trans-differentiation *in vitro* and *in vivo*[63]. hAMCs have a great ability to transdifferentiate into cardiomyocytes and to acquire immunologic tolerance *in vivo*, and are, therefore, a promising source of allograftable stem cells for cardiac regenerative medicine[63].

In dystrophic muscles, activated immune cell infiltrates (e.g., T lymphocytes and macrophages) are observed during the early stages of disease and play a critical role in muscle wasting[55-60]. Depletion or inhibition of these cells significantly improves dystrophic muscle pathology[64-66]. The findings of these studies suggest that much of the muscle damage that occurs when dystrophin is deficient is caused by inflammatory cells, as well as by direct mechanical damage.

Inflammatory cytokines, serum markers, and intramuscular nuclear factor-κB are not upregulated in a δ-sarcoglycan-deficient dystrophic hamster model following intramuscular injection of human- and pig-derived MSCs. Additionally, transplantation of these MSCs is associated with the formation of new muscle fibers and reduced muscular oxidative stress[67]. However, the majority of studies using MSCs in animal models do not report a significant, if any, increase in muscle contractile force[27]. The therapeutic effects of MSCs are believed to not only be owing to their differentiation in injured tissue, but also to their production of paracrine factors that inhibit apoptosis of injected cells, induce anti-inflammatory effects, and stimulate the

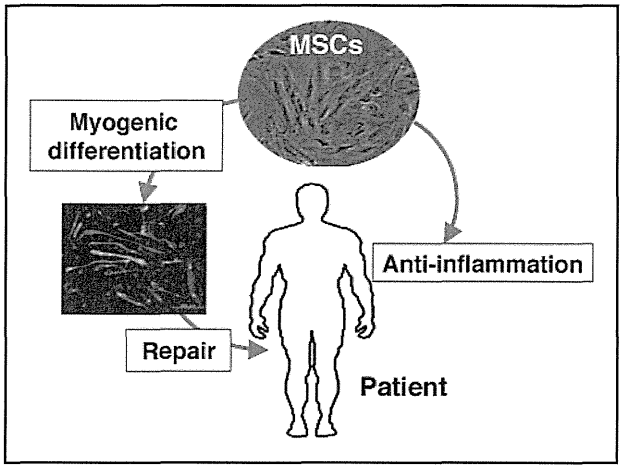

Fig.3 Cell-based therapeutic approach for muscular dystrophy
An approach to treat DMD using MSCs is shown. MSCs undergo myogenic differentiation and thereby contribute to muscle repair, and also elicit anti-inflammatory effects.

proliferation of endogenous stem cells at the site of injury.

Conclusion and future directions

Clinical interest in MSCs for cell therapeutic applications is based on their anti-inflammatory properties and their ability to release cytokines into the surrounding environment, thereby modifying the developmental fate of neighboring cells. In this review, we introduced various strategies for the engraftment of transplanted cells as a therapeutic approach for muscular dystrophies. MSCs are a promising therapy for muscle disease because they elicit immunosuppressive and/or anti-inflammatory effects and can undergo myogenic differentiation contributing to muscle repair (Fig.3).

Acknowledgements

We thank our colleagues, laboratory members, and collaborators at JCR Pharmaceuticals Co., Ltd. for their excellent experimental assistance and simulating discussions.

Sources of funding

A grant-in-aid for scientific research (KAKENHI), a grant from the National Center for Child Health and Development (24-1), and a research grant from JCR Pharmaceuticals Co., Ltd.

Disclosure of potential conflicts of interest

We have received research support from JCR Pharmaceuticals Co., Ltd. and TaKaRa Bio Inc.

References

1) Friedenstein AJ, Petrakova KV, Kurolesova AI, Frolova GP: Heterotopic of bone marrow. Analysis of precursor cells for osteogenic and hematopoietic tissues. Transplantation. 1968; 6: 230-247.
2) Zannettino AC, Paton S, Arthur A, Khor F, Itescu S, Gimble JM, Gronthos S: Multipotential human adipose-derived stromal stem cells exhibit a perivascular phenotype in vitro and in vivo. J Cell Physiol. 2008; 214: 413-421.
3) Hoogduijn MJ, Crop MJ, Peeters AM, Van Osch GJ, Balk AH, Ijzermans JN, Weimar W, Baan CC: Human heart, spleen, and perirenal fat-derived mesenchymal stem cells have immunomodulatory capacities. Stem Cells Dev. 2007; 16: 597-604.
4) Chao KC, Chao KF, Fu YS, Liu SH: Islet-like clusters derived from mesenchymal stem cells in Wharton's Jelly of the human umbilical cord for transplantation to control type 1 diabetes. PLoS One. 2008; 3: e1451.
5) Jo YY, Lee HJ, Kook SY, Choung HW, Park JY, Chung JH, Choung YH, Kim ES, Yang HC, Choung PH: Isolation and characterization of postnatal stem cells from human dental tissues. Tissue Eng. 2007; 13: 767-773.
6) He Q, Wan C, Li G: Concise review: multipotent mesenchymal stromal cells in blood. Stem Cells. 2007; 25: 69-77.
7) Oh W, Kim DS, Yang YS, Lee JK: Immunological properties of umbilical cord blood-derived mesenchymal stromal cells. Cell Immunol. 2008; 251: 116-123.
8) Meng X, Ichim TE, Zhong J, Rogers A, Yin Z, Jackson J, Wang H, Ge W, Bogin V, Chan KW, Thebaud B, Riordan NH: Endometrial regenerative cells: a novel stem cell population. J Transl Med. 2007; 5: 57.
9) Hida N, Nishiyama N, Miyoshi S, Kira S, Segawa K, Uyama T, Mori T, Miyado K, Ikegami Y, Cui C, Kiyono T, Kyo S, Shimizu T, Okano T, Sakamoto M, Ogawa S, Umezawa A: Novel cardiac precursor-like cells from human menstrual blood-derived mesenchymal cells. Stem Cells. 2008; 26: 1695-1704.
10) Patel AN, Park E, Kuzman M, Benetti F, Silva FJ, Allickson JG: Multipotent menstrual blood stromal stem cells: isolation, characterization, and differentiation. Cell Transplant. 2008; 17: 303-311.
11) Jazedje T, Perin PM, Czeresnia CE, Maluf M, Halpern S, Secco M, Bueno DF, Vieira NM, Zucconi E, Zatz M: Human fallopian tube: a new source of multipotent

adult mesenchymal stem cells discarded in surgical procedures. J Transl Med. 2009; 7: 46.
12) Bruder SP, Jaiswal N, Haynesworth SE: Growth kinetics, self-renewal, and the osteogenic potential of purified human mesenchymal stem cells during extensive subcultivation and following cryopreservation. J Cell Biochem. 1997; 64: 278-294.
13) Haynesworth SE, Goshima J, Goldberg VM, Caplan AI: Characterization of cells with osteogenic potential from human marrow. Bone. 1992; 13: 81-88.
14) Ju S, Teng GJ, Lu H, Jin J, Zhang Y, Zhang A, Ni Y: In vivo differentiation of magnetically labeled mesenchymal stem cells into hepatocytes for cell therapy to repair damaged liver. Invest Radiol. 2010; 45: 625-633.
15) Sun Y, Liu J, Qian F, Xu Q: Nitric oxide inhibits T cell adhesion and migration by down-regulation of beta1-integrin expression in immunologically liver-injured mice. Int Immunopharmacol. 2006; 6: 616-626.
16) Kopen GC, Prockop DJ, Phinney DG: Marrow stromal cells migrate throughout forebrain and cerebellum, and they differentiate into astrocytes after injection into neonatal mouse brains. Proc Natl Acad Sci U S A. 1999; 96: 10711-10716.
17) Ma Y, Xu Y, Xiao Z, Yang W, Zhang C, Song E, Du Y, Li L: Reconstruction of chemically burned rat corneal surface by bone marrow-derived human mesenchymal stem cells. Stem Cells. 2006; 24: 315-321.
18) Caplan AI, Bruder SP: Mesenchymal stem cells: building blocks for molecular medicine in the 21st century. Trends Mol Med. 2001; 7: 259-264.
19) Nauta AJ, Fibbe WE: Immunomodulatory properties of mesenchymal stromal cells. Blood. 2007; 110: 3499-3506.
20) Rasmusson I, Ringden O, Sundberg B, Le Blanc K: Mesenchymal stem cells inhibit the formation of cytotoxic T lymphocytes, but not activated cytotoxic T lymphocytes or natural killer cells. Transplantation. 2003; 76: 1208-1213.
21) Nitahara-Kasahara Y, Hayashita-Kinoh H, Ohshima-Hosoyama S, Okada H, Wada-Maeda M, Nakamura A, Okada T, Takeda S: Long-term engraftment of multipotent mesenchymal stromal cells that differentiate to form myogenic cells in dogs with Duchenne muscular dystrophy. Mol Ther. 2012; 20: 168-177.
22) Dezawa M, Ishikawa H, Itokazu Y, Yoshihara T, Hoshino M, Takeda S, Ide C, Nabeshima Y: Bone marrow stromal cells generate muscle cells and repair muscle degeneration. Science. 2005; 309: 314-317.
23) Mizuno H, Hyakusoku H: Mesengenic potential and future clinical perspective of human processed lipoaspirate cells. J Nippon Med Sch. 2003; 70: 300-306.
24) Bai L, Lennon DP, Eaton V, Maier K, Caplan AI, Miller SD, Miller RH: Human bone marrow-derived mesenchymal stem cells induce Th2-polarized immune response and promote endogenous repair in animal models of multiple sclerosis. Glia. 2009; 57: 1192-1203.
25) Wise CJ, Watt DJ, Jones GE: Conversion of dermal fibroblasts to a myogenic lineage is induced by a soluble factor derived from myoblasts. J Cell Biochem. 1996; 61: 363-374.
26) Chan J, O'Donoghue K, de la Fuente J, Roberts IA, Kumar S, Morgan JE, Fisk NM: Human fetal mesenchymal stem cells as vehicles for gene delivery. Stem Cells. 2005; 23: 93-102.
27) Gang EJ, Darabi R, Bosnakovski D, Xu Z, Kamm KE, Kyba M, Perlingeiro RC: Engraftment of mesenchymal stem cells into dystrophin-deficient mice is not accompanied by functional recovery. Exp Cell Res. 2009; 315: 2624-2636.
28) Quirici N, Soligo D, Bossolasco P, Servida F, Lumini C, Deliliers GL: Isolation of bone marrow mesenchymal stem cells by anti-nerve growth factor receptor antibodies. Exp Hematol. 2002; 30: 783-791.
29) Chen L, Tredget EE, Wu PY, Wu Y: Paracrine factors of mesenchymal stem cells recruit macrophages and endothelial lineage cells and enhance wound healing. PLoS One. 2008; 3: e1886.
30) Burdzinska A, Gala K, Paczek L: Myogenic stem cells. Folia Histochem Cytobiol. 2008; 46: 401-412.
31) Moser H: Duchenne muscular dystrophy: pathogenetic aspects and genetic prevention. Hum Genet. 1984; 66: 17-40.
32) Koenig M, Hoffman EP, Bertelson CJ, Monaco AP, Feener C, Kunkel LM: Complete cloning of the Duchenne muscular dystrophy (DMD) cDNA and preliminary genomic organization of the DMD gene in normal and affected individuals. Cell. 1987; 50: 509-517.
33) Campbell KP: Three muscular dystrophies: loss of cytoskeleton-extracellular matrix linkage. Cell. 1995; 80: 675-679.
34) Ervasti JM, Ohlendieck K, Kahl SD, Gaver MG, Campbell KP: Deficiency of a glycoprotein component of the dystrophin complex in dystrophic muscle. Nature.

1990; 345: 315-319.
35) Hahn A, Bach JR, Delaubier A, Renardel-Irani A, Guillou C, Rideau Y: Clinical implications of maximal respiratory pressure determinations for individuals with Duchenne muscular dystrophy. Arch Phys Med Rehabil. 1997; 78: 1-6.
36) Camargo FD, Green R, Capetanaki Y, Jackson KA, Goodell MA: Single hematopoietic stem cells generate skeletal muscle through myeloid intermediates. Nat Med. 2003; 9: 1520-1527.
37) Lee-Pullen TF, Bennett AL, Beilharz MW, Grounds MD, Sammels LM: Superior survival and proliferation after transplantation of myoblasts obtained from adult mice compared with neonatal mice. Transplantation. 2004; 78: 1172-1176.
38) Quenneville SP, Chapdelaine P, Rousseau J, Tremblay JP: Dystrophin expression in host muscle following transplantation of muscle precursor cells modified with the phiC31 integrase. Gene Ther. 2007; 14: 514-522.
39) Rodriguez AM, Pisani D, Dechesne CA, Turc-Carel C, Kurzenne JY, Wdziekonski B, Villageois A, Bagnis C, Breittmayer JP, Groux H, Ailhaud G, Dani C: Transplantation of a multipotent cell population from human adipose tissue induces dystrophin expression in the immunocompetent mdx mouse. J Exp Med. 2005; 201: 1397-1405.
40) De Bari C, Dell'Accio F, Vandenabeele F, Vermeesch JR, Raymackers JM, Luyten FP: Skeletal muscle repair by adult human mesenchymal stem cells from synovial membrane. J Cell Biol. 2003; 160: 909-918.
41) Goudenege S, Pisani DF, Wdziekonski B, Di Santo JP, Bagnis C, Dani C, Dechesne CA: Enhancement of myogenic and muscle repair capacities of human adipose-derived stem cells with forced expression of MyoD. Mol Ther. 2009; 17: 1064-1072.
42) Sampaolesi M, Blot S, D'Antona G, Granger N, Tonlorenzi R, Innocenzi A, Mognol P, Thibaud JL, Galvez BG, Barthelemy I, Perani L, Mantero S, Guttinger M, Pansarasa O, Rinaldi C, Cusella De Angelis MG, Torrente Y, Bordignon C, Bottinelli R, Cossu G: Mesoangioblast stem cells ameliorate muscle function in dystrophic dogs. Nature. 2006; 444: 574-579.
43) Wang Z, Chamberlain JS, Tapscott SJ, Storb R: Gene therapy in large animal models of muscular dystrophy. ILAR J. 2009; 50: 187-198.
44) Ramirez M, Lucia A, Gomez-Gallego F, Esteve-Lanao J, Perez-Martinez A, Foster C, Andreu AL, Martin MA, Madero L, Arenas J, Garcia-Castro J: Mobilisation of mesenchymal cells into blood in response to skeletal muscle injury. Br J Sports Med. 2006; 40: 719-722.
45) Koc ON, Gerson SL, Cooper BW, Dyhouse SM, Haynesworth SE, Caplan AI, Lazarus HM: Rapid hematopoietic recovery after coinfusion of autologous-blood stem cells and culture-expanded marrow mesenchymal stem cells in advanced breast cancer patients receiving high-dose chemotherapy. J Clin Oncol. 2000; 18: 307-316.
46) Schenk S, Mal N, Finan A, Zhang M, Kiedrowski M, Popovic Z, McCarthy PM, Penn MS: Monocyte chemotactic protein-3 is a myocardial mesenchymal stem cell homing factor. Stem Cells. 2007; 25: 245-251.
47) Seeger FH, Zeiher AM, Dimmeler S: Cell-enhancement strategies for the treatment of ischemic heart disease. Nat Clin Pract Cardiovasc Med. 2007; 4 Suppl 1: S110-S113.
48) Shyu WC, Lee YJ, Liu DD, Lin SZ, Li H: Homing genes, cell therapy and stroke. Front Biosci. 2006; 11: 899-907.
49) Voermans C, van Hennik PB, van der Schoot CE: Homing of human hematopoietic stem and progenitor cells: new insights, new challenges? J Hematother Stem Cell Res. 2001; 10: 725-738.
50) Pierdomenico L, Bonsi L, Calvitti M, Rondelli D, Arpinati M, Chirumbolo G, Becchetti E, Marchionni C, Alviano F, Fossati V, Staffolani N, Franchina M, Grossi A, Bagnara GP: Multipotent mesenchymal stem cells with immunosuppressive activity can be easily isolated from dental pulp. Transplantation. 2005; 80: 836-842.
51) Di Nicola M, Carlo-Stella C, Magni M, Milanesi M, Longoni PD, Matteucci P, Grisanti S, Gianni AM: Human bone marrow stromal cells suppress T-lymphocyte proliferation induced by cellular or nonspecific mitogenic stimuli. Blood. 2002; 99: 3838-3843.
52) Kerkis I, Ambrosio CE, Kerkis A, Martins DS, Zucconi E, Fonseca SA, Cabral RM, Maranduba CM, Gaiad TP, Morini AC, Vieira NM, Brolio MP, Sant'Anna OA, Miglino MA, Zatz M: Early transplantation of human immature dental pulp stem cells from baby teeth to golden retriever muscular dystrophy (GRMD) dogs: Local or systemic? J Transl Med. 2008; 6: 35.
53) Newman RE, Yoo D, LeRoux MA, Danilkovitch-

Miagkova A: Treatment of inflammatory diseases with mesenchymal stem cells. Inflamm Allergy Drug Targets. 2009; 8: 110-123.

54) Spaggiari GM, Abdelrazik H, Becchetti F, Moretta L: MSCs inhibit monocyte-derived DC maturation and function by selectively interfering with the generation of immature DCs: central role of MSC-derived prostaglandin E2. Blood. 2009; 113: 6576-6583.

55) Yang YW, Bai H, Wang CB, Lin M, Wu LQ: [Experimental study on influence of bone marrow mesenchymal stem cells on activation and function of mouse peritoneal macrophages]. Zhonghua Xue Ye Xue Za Zhi. 2008; 29: 540-543.

56) Chen L, Zhang W, Yue H, Han Q, Chen B, Shi M, Li J, Li B, You S, Shi Y, Zhao RC: Effects of human mesenchymal stem cells on the differentiation of dendritic cells from CD34+ cells. Stem Cells Dev. 2007; 16: 719-731.

57) Selmani Z, Naji A, Zidi I, Favier B, Gaiffe E, Obert L, Borg C, Saas P, Tiberghien P, Rouas-Freiss N, Carosella ED, Deschaseaux F: Human leukocyte antigen-G5 secretion by human mesenchymal stem cells is required to suppress T lymphocyte and natural killer function and to induce CD4+CD25 high FOXP3+ regulatory T cells. Stem Cells. 2008; 26: 212-222.

58) Casiraghi F, Azzollini N, Cassis P, Imberti B, Morigi M, Cugini D, Cavinato RA, Todeschini M, Solini S, Sonzogni A, Perico N, Remuzzi G, Noris M: Pretransplant infusion of mesenchymal stem cells prolongs the survival of a semiallogeneic heart transplant through the generation of regulatory T cells. J Immunol. 2008; 181: 3933-3946.

59) Le Blanc K, Rasmusson I, Sundberg B, Gotherstrom C, Hassan M, Uzunel M, Ringden O: Treatment of severe acute graft-versus-host disease with third party haploidentical mesenchymal stem cells. Lancet. 2004; 363: 1439-1441.

60) Fang B, Song YP, Liao LM, Han Q, Zhao RC: Treatment of severe therapy-resistant acute graft-versus-host disease with human adipose tissue-derived mesenchymal stem cells. Bone Marrow Transplant. 2006; 38: 389-390.

61) Holladay CA, Duffy AM, Chen X, Sefton MV, O'Brien TD, Pandit AS: Recovery of cardiac function mediated by MSC and interleukin-10 plasmid functionalised scaffold. Biomaterials. 2012; 33: 1303-1314.

62) Min CK, Kim BG, Park G, Cho B, Oh IH: IL-10-transduced bone marrow mesenchymal stem cells can attenuate the severity of acute graft-versus-host disease after experimental allogeneic stem cell transplantation. Bone Marrow Transplant. 2007; 39: 637-645.

63) Tsuji H, Miyoshi S, Ikegami Y, Hida N, Asada H, Togashi I, Suzuki J, Satake M, Nakamizo H, Tanaka M, Mori T, Segawa K, Nishiyama N, Inoue J, Makino H, Miyado K, Ogawa S, Yoshimura Y, Umezawa A: Xenografted human amniotic membrane-derived mesenchymal stem cells are immunologically tolerated and transdifferentiated into cardiomyocytes. Circ Res. 2010; 106: 1613-1623.

64) Cai B, Spencer MJ, Nakamura G, Tseng-Ong L, Tidball JG: Eosinophilia of dystrophin-deficient muscle is promoted by perforin-mediated cytotoxicity by T cell effectors. Am J Pathol. 2000; 156: 1789-1796.

65) Hodgetts S, Radley H, Davies M, Grounds MD: Reduced necrosis of dystrophic muscle by depletion of host neutrophils, or blocking TNFalpha function with Etanercept in mdx mice. Neuromuscul Disord. 2006; 16: 591-602.

66) Radley HG, Grounds MD: Cromolyn administration (to block mast cell degranulation) reduces necrosis of dystrophic muscle in mdx mice. Neurobiol Dis. 2006; 23: 387-397.

67) Shabbir A, Zisa D, Leiker M, Johnston C, Lin H, Lee T: Muscular dystrophy therapy by nonautologous mesenchymal stem cells: muscle regeneration without immunosuppression and inflammation. Transplantation. 2009; 87: 1275-1282.

nature COMMUNICATIONS

ARTICLE

Received 1 Jul 2014 | Accepted 13 Oct 2014 | Published 24 Nov 2014

DOI: 10.1038/ncomms6551

Reward-timing-dependent bidirectional modulation of cortical microcircuits during optical single-neuron operant conditioning

Riichiro Hira[1,2], Fuki Ohkubo[1,2], Yoshito Masamizu[1,2], Masamichi Ohkura[3], Junichi Nakai[3], Takashi Okada[4] & Masanori Matsuzaki[1,2]

Animals rapidly adapt to environmental change. To reveal how cortical microcircuits are rapidly reorganized when an animal recognizes novel reward contingency, we conduct two-photon calcium imaging of layer 2/3 motor cortex neurons in mice and simultaneously reinforce the activity of a single cortical neuron with water delivery. Here we show that when the target neuron is not relevant to a pre-trained forelimb movement, the mouse increases the target neuron activity and the number of rewards delivered during 15-min operant conditioning without changing forelimb movement behaviour. The reinforcement bidirectionally modulates the activity of subsets of non-target neurons, independent of distance from the target neuron. The bidirectional modulation depends on the relative timing between the reward delivery and the neuronal activity, and is recreated by pairing reward delivery and photoactivation of a subset of neurons. Reward-timing-dependent bidirectional modulation may be one of the fundamental processes in microcircuit reorganization for rapid adaptation.

[1] Division of Brain Circuits, National Institute for Basic Biology and the Graduate University of Advanced Studies (Sokendai), Myodaiji, Okazaki, Japan. [2] Japan Science and Technology Agency, CREST, Saitama 332-0012, Japan. [3] Brain Science Institute, Saitama University, Saitama 338-8570, Japan. [4] Department of Biochemistry and Molecular Biology, Nippon Medical School, Tokyo 113-8602, Japan. Correspondence and requests for materials should be addressed to M.M. (email: mzakim@nibb.ac.jp).

Animals can rapidly adapt to environmental changes. This is accomplished by the reorganization of neuronal activity. When the adaptation requires body movement, activity changes occur in many motor cortex neurons associated with motor commands and proprioceptive feedback[1]. By contrast, when the adaptation does not require body movement and the cortical activity is reinforced with repeated reward deliveries, primates can volitionally control the cortical activity at the level of single neurons[1–5]. Single-neuron operant conditioning (SNOC) provides a framework for studying the reorganization of neuronal activity during rapid adaptation because it is accompanied by modulation of the activity of non-target neurons, and the associations between non-target and target neurons can be unambiguously determined. Theoretically, cortical reorganization during both SNOC and brain-machine and brain-computer interface learning can be explained by reward-timing-dependent plasticity, in which the activity change in an individual neuron depends on the activity timing relative to a global reward signal[6–8]. In addition to the inputs associated with the global reward signal, cortical neurons receive strong synaptic inputs from surrounding neurons. Consistent with this, non-target neurons whose activity is highly correlated with that of the target neuron tend to change their firing rate with the target neuron[9,10]. However, individual neurons recorded from the same electrode can be separately controlled in SNOC[2,3,9,11]. It is difficult to determine the spatial and temporal modulation in cortical activity in fine-scale ($<500\,\mu m$) microcircuits using electrical recordings.

Two-photon calcium imaging of cortical neurons has been used to identify multineuronal activity within a motor cortical microcircuit in rodents[12–16]. In contrast to SNOC in the primate, SNOC in the rodent[11,17] has not been performed with identification of the relations of individual neurons to physical movement. Here, we pre trained mice to perform a lever-pull movement using the right forelimb to obtain water. Then, we conducted two-photon calcium imaging of multiple neurons in layer 2/3 (L2/3) motor forelimb areas and determined whether individual neurons were related to lever-pull movement or not. Immediately after that, we conditioned the mice by reinforcing the calcium transients of a single target neuron, but not the lever-pull movement, with water delivery (SNOC by two-photon calcium imaging; 2pSNOC). We found that when the target neuron was not related to the lever-pull movement, the activity of the target neuron rapidly increased during 15 min of 2pSNOC. This increase was not accompanied by an increase in the frequency of lever-pull movements. During 2pSNOC, a subset of non-target neurons that showed high activity synchronous with reward delivery increased their activity, whereas a subset that showed high activity 2–4 s after reward delivery decreased their activity. This upward and downward modulation was recreated by repetitive channelrhodopsin-2 (ChR2) photostimulation[18] of neurons 250 ms before and 2.5 s after the reward delivery, respectively. The results indicate that reward-timing-dependent bidirectional modulation is a fundamental process in L2/3 microcircuit reorganization during fast adaptation to novel environments.

Results

Physical and neuronal operant conditioning. To introduce physical operant conditioning before 2pSNOC, head-restrained mice were trained to perform a self-initiated lever-pull task using the right forelimb[13,16,19]. A 4-μl water drop was provided as a reward when the lever was pulled for 0.4 s after being left in the wait position for >3 s (Fig. 1a)[13]. An adeno-associated virus (AAV) encoding a calcium indicator, GCaMP7[20], was injected into the left motor forelimb areas[13,21,22] 1–2 weeks before the start of the lever-pull task-training sessions. After 5–14 lever-pull task-training sessions (one session per day), two-photon calcium imaging of L2/3 motor cortical neurons was performed while mice performed 2pSNOC. A total of 24 2pSNOC sessions were recorded in seven mice (one to eight sessions per mouse). Each 2pSNOC session consisted of three periods (Fig. 1b): a pre-conditioning period (10 min), a conditioning period (15 min) and a post-conditioning period (10 min). 2pSNOC was performed during the conditioning period.

The pre-conditioning period was used to classify the imaged neurons according to their association with the pre-trained lever-pull movement and to select a conditioned neuron (target neuron). Mice could freely pull the lever, but the reward corresponding to a successful lever-pull for the lever-pull task (>0.4 s pull with >3 s wait) was omitted to avoid satiation. A successful lever-pull that did not directly induce the reward was defined as a virtual hit. Virtual hits occurred at a frequency of $1.9 \pm 0.1\,min^{-1}$ during the pre-conditioning period ($n = 24$ sessions from seven mice), possibly because of partial habituation and/or expectation of reward. Many neurons exhibited large calcium transients related to the lever-pull movement, similar to our previous report[13]. According to the value of normalized non-negative deconvolution[23] of each relative fluorescent change ($\Delta F/F$) trace ('activity'; see Methods), active neurons during the pre-conditioning period were reconstructed (35.0 ± 16.4 neurons, $n = 24$ sessions from seven mice) and classified into two groups: neurons with high activity during lever-related periods (from 1 s before the onset of lever-pull to 3 s after the end of lever-pull; 'lever-related neurons') (Fig. 1c), and other neurons ('lever-unrelated neurons') (Fig. 1d). Most reconstructed neurons were assumed to be excitatory neurons because GCaMP expression was under the control of synapsin I promoter, which considerably limits the expression to excitatory neurons[16,24]. One neuron was targeted in the conditioning period. This target neuron was a lever-related neuron in 13 sessions and a lever-unrelated neuron in 11 sessions.

During the conditioning period, the mouse performed a 2pSNOC task. During the 2pSNOC task, two 4-μl water drops were delivered to the mouse immediately after the $\Delta F/F$ of a single target neuron increased above a threshold (Fig. 1a,e–g). A water reward was delivered after a calcium transient in the target neuron, irrespective of whether the target neuron was lever-related or lever-unrelated (Fig. 1c,d). Calcium transients in nearby neurons did not trigger reward delivery (Fig. 1f,g). Ninety-eight percent of the water rewards were given immediately after the calcium transient in the target neuron exceeded the threshold (1,000 successful rewards from 1,020 total rewards in 24 sessions from seven mice). The remaining 2% of rewards were delivered when $\Delta F/F$ exceeded the threshold without an obvious calcium transient. The latency from the calcium transient in the target neuron to the corresponding reward delivery was 212 ± 122 ms ($n = 1{,}000$ successful rewards), which, when compared with values reported in a previous study, was sufficiently fast for operant conditioning[25].

Rapid activity changes in target neurons during SNOC. First, we examined whether reward delivery corresponding to calcium transients in lever-related and lever-unrelated target neurons resulted in rapid changes in the activity of the target neuron during the 15 min conditioning period. For lever-unrelated target neurons, activity increased by ~50%, whereas, for lever-related target neurons, activity did not change (Fig. 2a,b). Activity gain was defined as the ratio of the mean activity in the last 5 min of the conditioning period (late conditioning period) to the mean activity in the first 5 min of the conditioning period (early

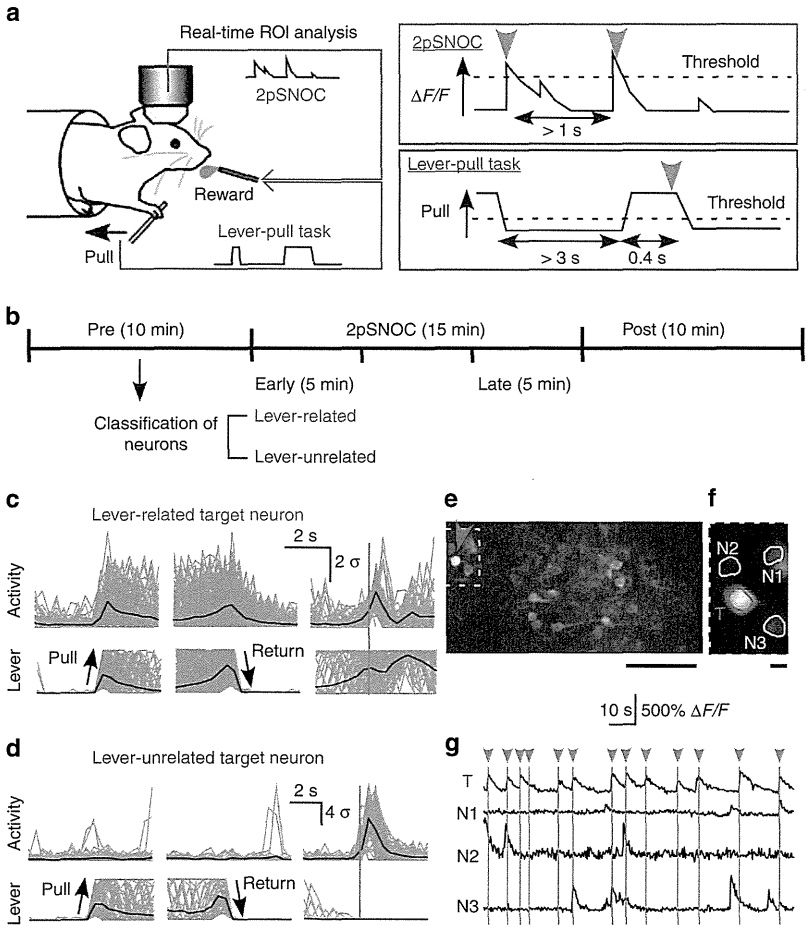

Figure 1 | Single-neuron operant conditioning. (**a**) A head-restrained mouse was provided with a water reward every time a calcium transient in the target neuron exceeded a threshold (2pSNOC task, top right; red) or every time the mouse successfully pulled a lever (lever-pull task, bottom right; grey). In the 2pSNOC task, one computer controlled two-photon imaging and another was used to analyze fluorescence intensity of a region of interest (ROI) containing a target neuron and control water delivery. Cyan arrowheads denote reward delivery. (**b**) The timeline for a 2pSNOC session showing the three imaging periods. (**c**,**d**) Activity of a representative lever-related target neuron (**c**) and a representative lever-unrelated target neuron (**d**) aligned to lever-pull onset (left), lever-return end (middle) and reward delivery (vertical cyan bar, right) during all three imaging periods. The lever trajectory is shown below the neuron activity. The thick black traces denote the mean of all traces. (**e**) A time-averaged image of a representative L2/3 field during the 2pSNOC task. Red arrowhead indicates the target neuron. Scale bar, 100 μm. (**f**) Expanded image of the rectangle in panel **e**. ROIs for the target neuron (T) and three neighboring neurons (N1, N2 and N3) are overlaid. Scale bar, 10 μm. (**g**) Relative change in fluorescence ($\Delta F/F$) of the target neuron and the three neighboring neurons shown in panel **f** during the 2pSNOC task. Vertical cyan bars denote reward delivery.

conditioning period) minus 1. When activity gain was averaged across sessions and/or neurons, the logarithmic mean of the ratio was used (Fig. 2c). For lever-unrelated target neurons, the activity gain was substantially above zero (Fig. 2d and Table 1). For lever-related target neurons, activity gain was not different from zero (Fig. 2d and Table 1). This pattern remained even after exclusion of the mouse in which eight sessions were performed, with a mean activity gain of 55.3% and −0.73% in lever-unrelated and lever-related target neurons, respectively.

Next, we determined whether operant conditioning of the target neuron increased the frequency of reward delivery induced by calcium transients above the threshold. As expected, the reward frequency increased by ~50% when lever-unrelated neurons were targeted, and did not change when lever-related neurons were targeted (Fig. 3a). Similar to activity gain, reward gain was defined as the ratio of the reward frequency in the late conditioning period to the reward frequency in the early conditioning period minus 1, and the logarithmic mean of the ratio was used for averaging (Fig. 3b). The reward gain was substantially above zero when lever-unrelated neurons were targeted, and was not different from zero when lever-related neurons were targeted (Fig. 3c). The activity gain and the reward gain were correlated in both types of target neurons (Fig. 3d). When lever-unrelated neurons were targeted, activity gain was positive in all 11 sessions (from five mice) and reward gain was positive in 8 of the 11 sessions; therefore, the mouse steadily increased the target neuron activity and reward frequency.

Next, we examined the specificity of the target neuron. The mean activity gain of the non-target neurons was slightly larger than zero when a lever-unrelated neuron was targeted and slightly smaller than zero when a lever-related neuron was targeted (Table 2). To examine whether the relative change in activity of the target neuron from the early to the late conditioning period exceeded that in the non-target neurons, we ranked the activity of the target neuron among all reconstructed neurons, including target and non-target neurons. The rank was normalized between

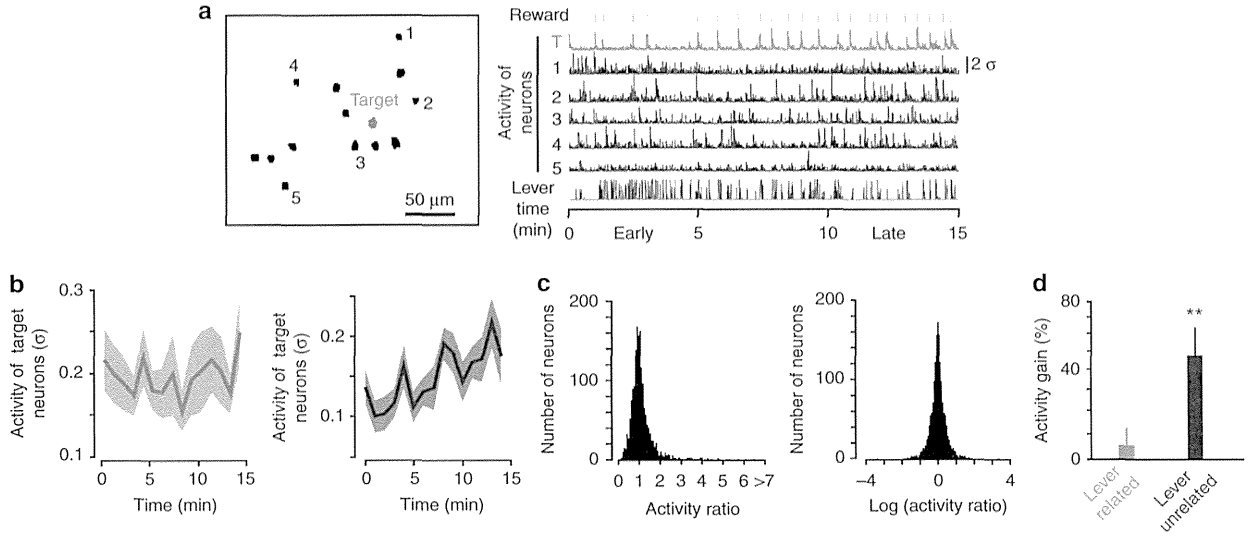

Figure 2 | Neuronal activity during optical single-neuron operant conditioning. (**a**) Left, an example of the imaged field. T (red) indicates the lever-unrelated target neuron. Black indicates the non-target neurons that were simultaneously monitored. Right, non-negatively deconvoluted $\Delta F/F$ (activity) of the target neuron and five representative non-target neurons during the 15-min conditioning period. The activity is Z scored for each neuron. Vertical cyan bars denote reward delivery. (**b**) Time course of the activity of lever-related (left; $n=13$) and lever-unrelated (right; $n=11$) target neurons during the conditioning period. The activity is Z scored for each neuron. Thick lines and shading indicate the mean ± s.e.m. (**c**) Left, a histogram of the activity ratio from all reconstructed neurons ($n=840$ from 24 sessions from seven mice), where the activity ratio for each neuron was calculated as the mean activity in the first 5 min of the conditioning period divided by that in the last 5 min of the conditioning period or the mean activity in the last 5 min divided by that in the first 5 min. When all activity ratios were summed and then divided by the number of neurons, the mean value was 1.13; significantly larger than one ($P<10^{-8}$, t-test). Thus, if the linear sum of the activity ratio divided by the neuron number is used as the mean, the mean is positive. Right, a histogram of the log-scaled activity ratio. The mean was zero by definition and the s.d. was 0.46. Thus, the logarithmic mean of the ratio of the mean activity in the last 5 min divided by that in the early 5 min was used for averaging. (**d**) Activity gain of lever-related and lever-unrelated target neurons (lever-related, $P=0.43$, $n=13$; lever-unrelated, $^{**}P=0.0039$, $n=11$; one-sample t-test compared with zero).

Table 1 | The mean activity gain of each type of target neuron.

Target neuron	Mean activity gain (%)	*P* value	Number of neurons
Lever related	5.6	0.43	13
Lever unrelated	47.4	0.0039	11

The mean activity gain of lever-related and lever-unrelated target neurons. In each type of neuron, *P* value was obtained by one-sample *t*-test compared with zero.

1 (top) and 100 (bottom) in the early and late conditioning periods during each session. When a lever-unrelated neuron was targeted, the normalized rank of the target neuron significantly rose from the early to the late conditioning period (change in normalized rank, 18.0 ± 6.4; $P=0.0078$, Wilcoxon signed-rank test; $n=11$). When a lever-related neuron was targeted, the normalized rank of the target neuron was similar in the early and late conditioning periods (change in normalized rank, 4.5 ± 4.1; $P=0.56$, Wilcoxon signed-rank test; $n=13$). Thus, both of the activity and rank of the target neuron significantly increased from the early to the late conditioning period when a lever-unrelated neuron was targeted. These results indicate that the rapid operant conditioning of single lever-unrelated neurons was successful even though the activity of non-target neurons slightly changed. By contrast, the rapid operant conditioning of single lever-related neurons was not successful.

In lever-related neurons, calcium transients would coincide with a lever-pull. In the 2pSNOC, mice were rewarded for calcium transients in the target neuron. Therefore, when lever-related neurons were targeted, pulling the lever would result in the delivery of a reward, meaning that the mice did not have to change the strategy that they adopted in the lever-pull task to get rewards during the conditioning period. In support of this, the amount of time spent pulling the lever and the frequency of virtual hits in the conditioning period were approximately twofold larger when lever-related neurons were targeted than when lever-unrelated neurons were targeted (Fig. 3e,f), although licking frequency was not different (Fig. 3g). Irrespective of the target neuron type, lever-pull behaviours did not change from the early to the late conditioning period. These results suggest that, when lever-related neurons were targeted, the mouse performed goal-directed lever-pull movements from the onset of the conditioning period without recognition of SNOC. This may explain why the activity gain for lever-related target neurons was not significantly positive. In the following analyses of the microcircuit reorganization during 2pSNOC, only data from sessions with a lever-unrelated target neuron were used (11 sessions from five mice; $n=381$ non-target neurons).

Reward-timing-dependent bidirectional modulation. Next, we examined whether non-target neurons associated with the target neuron changed their activity more markedly than other non-target neurons. The activity gain was similar for lever-related non-target neurons and lever-unrelated non-target neurons (Fig. 4a and Table 2). The activity gain of non-target neurons was not associated with the distance to the target neuron (Fig. 4b). By contrast, the activity gain of non-target neurons was weakly related to the pairwise correlation with the target neuron during the conditioning period (excluding the reward-related periods

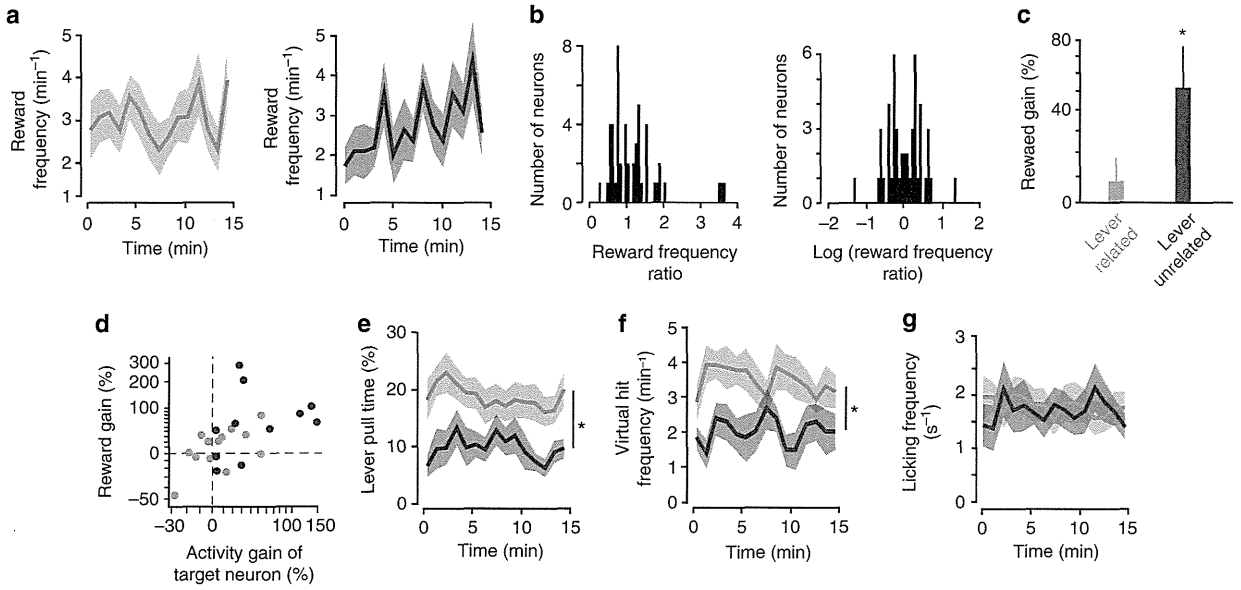

Figure 3 | Reward frequency and behaviours during optical single-neuron operant conditioning. (**a**) Time course of the reward frequency when lever-related (left; $n=13$) and lever-unrelated (right; $n=11$) neurons were targeted. Thick lines and shading indicate the mean ± s.e.m. (**b**) Left, a histogram of the reward frequency ratio from all sessions ($n=24$ sessions from seven mice), where the reward frequency ratio was calculated as the mean reward frequency in the first 5 min divided by that in the last 5 min or the mean reward frequency in the last 5 min divided by that in the first 5 min. Right, a histogram of the log-scaled reward frequency ratio. (**c**) Reward gain when lever-related and lever-unrelated neurons were targeted (lever-related, $P=0.37$, $n=13$; lever-unrelated, $^*P=0.020$, $n=11$; one-sample t-test compared with zero). (**d**) The reward gain as a function of the activity gain of the target neurons. Each circle indicates a different session. Magenta, lever-related target neurons. Blue, lever-unrelated target neurons. (Pearson's correlation coefficient = 0.54, $P=0.0065$, $n=24$ sessions). (**e**) Time course of the percentage of time spent pulling the lever when lever-related (magenta, $n=13$) and lever-unrelated (blue, $n=11$) neurons were targeted. Thick lines and shading indicate the mean ± s.e.m. $^*P=0.011$; Wilcoxon rank sum test. (**f**) Time course of the frequency of virtual hits when lever-related (magenta $n=13$) and lever-unrelated (blue $n=11$) neurons were targeted. Thick lines and shading indicate the mean ± s.e.m. $^*P=0.013$; Wilcoxon rank sum test. (**g**) Time course of the frequency of licking when lever-related (magenta, $n=13$) and lever-unrelated (blue, $n=11$) neurons were targeted. Thick lines and shading indicate the mean ± s.e.m.

Table 2 | The mean activity gain of each type of non-target neuron.

Type of target neuron	Type of non-target neuron	Mean activity gain (%)	*P* value	Number of non-target neurons
Lever related	Lever related	−5.3	0.0019	364
	Lever unrelated	0.6	0.89	71
	Sum of the two types	−4.3	0.006	435
Lever unrelated	Lever related	7.0	0.042	226
	Lever unrelated	9.1	0.076	155
	Sum of the two types	7.9	0.0071	381

The mean activity gain of lever-related and lever-unrelated non-target neurons and their sum when a lever-related neuron was targeted ($n=13$ sessions) or when a lever-unrelated neuron was targeted ($n=11$ sessions). In each type of neuron, *P* value was obtained by one-sample t-test compared with zero.

from 0 to 5 s after each reward delivery; spontaneous pairwise correlation) (Fig. 4c). This indicates that non-target neurons whose activity was temporally, but not spatially, associated with the target neuron increased their activity, although the strength of the spontaneous pairwise correlation was negatively associated with the cellular distance (Fig. 4d), as previously reported in the mouse motor cortex[12,13,15].

Although the change in the activity of non-target neurons was weakly associated with the correlation with the target neuron, non-target neurons should have been affected by the water delivery because it was the reinforcer. Therefore, we next investigated whether the activity gain was affected by the activity timing of the non-target neurons relative to the reward delivery (Fig. 5a). For each non-target neuron, the ratio of the sum of the activity in a 0.33-s time bin t s after reward delivery during the first 10 min of the conditioning period to the sum of the remaining activity in the same bin during the first 10 min of the conditioning period was defined as the reward synchronization index (t) (RSI(t); see Methods for details). For each time bin, activity gain was averaged across the non-target neurons with RSI values in the top 5% (Fig. 5b). The activity gain of non-target neurons with RSI in the top 5% was significantly larger than zero when t ranged from −0.33 s to 0.33 s, and significantly smaller than zero when t was 2.3, 3 and 4 s (Fig. 5c). We refer to this phenomenon as reward-timing-dependent bidirectional modulation (RTBM), and refer to neurons that had at least one RSI (−0.33 s to 0.33 s) in the top 5% as reward-synchronous active (SR) neurons ($n=34$) and neurons that had at least one RSI (2–4 s) in the top 5% as after-reward active (AR) neurons ($n=39$). Neurons that met both criteria were categorized according to the time bin with the highest RSI. The activity gain of SR and AR neurons was substantially positive and negative, respectively (Fig. 5d). RTBM was also detected when RSI values that determined SR and AR neurons ranged from the top 2% to the top 10% (Fig. 5e). In addition, RTBM was observed when neurons with RSI in the top 20% for each time

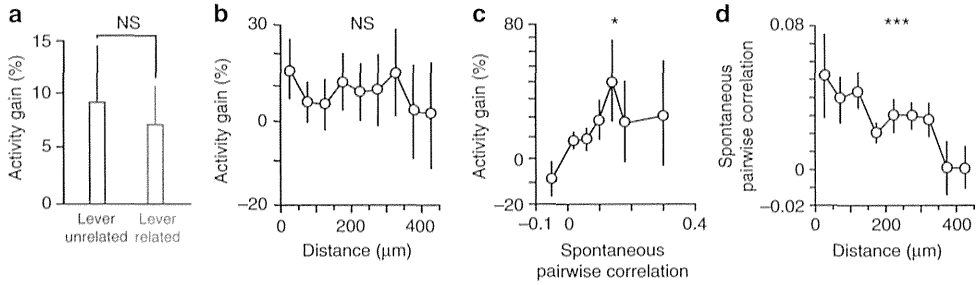

Figure 4 | Modulation of non-target neurons. (**a**) Activity gain of lever-unrelated (blue, $n=226$) and lever-related (magenta, $n=155$) non-target neurons. NS indicates no significant difference ($P=0.74$; two-sample t-test). (**b**) Activity gain of non-target neurons as a function of the distance from the target neuron (Spearman's correlation coefficient $(r)=-0.0077$, $P=0.88$, $n=381$). (**c**) Activity gain of non-target neurons as a function of the strength of the spontaneous pairwise correlation with the target neuron during the conditioning period ($r=0.10$, $^{*}P=0.043$, $n=381$). (**d**) Strength of the spontaneous pairwise correlation between each non-target neuron and the target neuron during the conditioning period as a function of distance between the two neurons ($r=-0.22$, $^{***}P=1.8\times10^{-5}$, $n=381$).

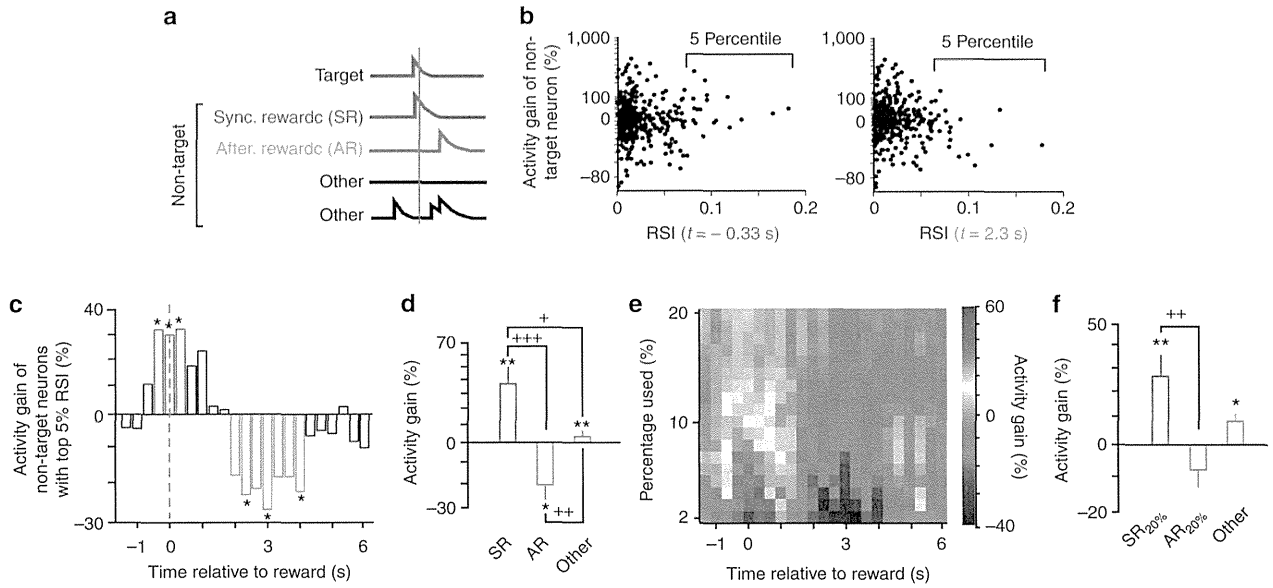

Figure 5 | Reward-timing-dependent bidirectional modulation. (**a**) Activity of target neurons (red), non-target neurons with high activity around reward delivery (green) or after reward delivery (orange) and other non-target neurons (black). (**b**) Activity gain of non-target neurons as a function of the reward synchronization index (RSI) at 0.33 s before (left) and 2.3 s after (right) reward delivery. (**c**) Mean activity gain of non-target neurons with RSI in the top 5% as a function of the RSI time bin. Vertical cyan dashed line denotes reward timing. Asterisks indicate $P<0.05$ (one-sample t-test compared with zero). Green and orange bars indicate the time bins used to determine reward-synchronous active (SR) and after-reward active (AR) neurons, respectively. (**d**) Mean activity gain of SR, AR and other non-target neurons. SR, $P=0.0017$, $n=34$; AR, $P=0.010$, $n=39$; other non-target, $P=0.0014$, $n=308$; one-sample t-test compared with zero. $^{*}P<0.05$, $^{**}P<0.01$. One-way ANOVA indicated a significant difference across neuron types ($P=6.7\times10^{-5}$). $^{+}P=0.049$, $^{++}P=0.0014$, $^{+++}P=4.1\times10^{-5}$; *post-hoc* HSD test. (**e**) Mean activity gain of non-target neurons with the top 2–20% RSI from the pooled data as a function of the RSI time bin relative to reward delivery. The activity gain is pseudo-colour coded. (**f**) Mean activity gains of $SR_{20\%}$, $AR_{20\%}$ and other non-target neurons, where non-target neurons with the top 20% RSI ($t=0$ s and $t=2.3$ s) in each session were defined as $SR_{20\%}$ neurons (green) and $AR_{20\%}$ neurons (orange), respectively ($SR_{20\%}$, $^{**}P=0.0026$, $n=74$; $AR_{20\%}$, $P=0.19$, $n=74$; the other non-target neurons, $^{*}P=0.021$, $n=233$, one-sample t-test compared with zero). The activity gain of $SR_{20\%}$ neurons was significantly larger than that of $AR_{20\%}$ neurons ($P=0.0022$, one-way ANOVA, $^{++}P=0.0013$, *post hoc* HSD test).

bin in each session were selected; the activity gain of neurons with RSI (0 s) in the top 20% ($SR_{20\%}$ neurons) averaged across-sessions was substantially higher than zero and that of neurons with RSI (2.3 s) in the top 20% ($AR_{20\%}$ neurons) averaged across-sessions (Fig. 5f). In 9 of 10 sessions with >2 $SR_{20\%}$ neurons and >2 $AR_{20\%}$ neurons (five, two, one, and one out of five, two, two and one sessions from four mice, respectively), the mean activity gain of $SR_{20\%}$ neurons was higher than that of $AR_{20\%}$ neurons; thus, the timing of neuronal activity relative to the reward was a critical factor in the modulation of the two groups of non-target neurons.

We next examined the association between SR and AR neurons and the target neuron. The percentage of lever-related and lever-unrelated neurons was similar between SR and AR neurons (Fig. 6a) and the distance of SR and AR neurons from the target neuron was similar to the distance of other neurons from the target neuron (Fig. 6b). The pairwise correlation with the target neuron was higher for SR neurons than for AR neurons and other neurons

during both the conditioning and pre-conditioning periods, that is, without water delivery (Fig. 6c). This is consistent with the result shown in Fig. 4c and indicates that SR neurons were frequently active together with the target neuron because the reward delivery was induced by a calcium transient in the target neuron beyond the threshold with only ~200 ms delay. Thus, SR neurons, which were highly correlated with the target neuron, exhibited an increase in activity irrespective of whether the activity was lever-related, or the distance from the target neuron. By contrast, AR neurons did not appear different from other non-target neurons in terms of their associations with the target neuron.

Neither SR nor AR neurons were specifically related to licking because licking frequency around the reward (-1 to 1 s) or after the reward (2 to 4 s) did not change from the early to the late conditioning period (Fig. 7a). Likewise, neither SR nor AR neurons were specifically related to lever-pull in response to the reward delivery because the percentage of lever-pull time and the probability of lever pulling around the reward (-1 to 1 s) and after the reward (2 to 4 s) did not change from the early to the late conditioning period (Fig. 7b,c). Therefore, the activity changes in AR or SR neurons cannot be explained by a gradual loss of the pre-trained memory for the mouse to pull the lever 3 s after the reward delivery.

We also estimated whether reward-related activity accounted for the activity gain of SR and AR neurons. The reward-related activity index (RRAI) was defined as the mean activity during the reward-related period divided by the mean activity during the non-reward-related periods of the conditioning period. Reward-related neurons were defined as the neurons with the top 5% of RRAI values because these neurons contributed to the skewed distribution of RRAI (Fig. 7d). As expected, the reward-related neurons tended to have positive activity gain (27.0%, $P=0.14$, $n=19$, one-sample t-test). The proportion of SR and AR neurons that were reward related was similar (14.8% for SR neurons, 23.1% for AR neurons; $P=0.36$, χ^2-test). The proportion of lever-related and lever-unrelated neurons that were reward related was also similar (5.8% for lever-related neurons, 3.9% for lever-unrelated neurons; $P=0.41$, χ^2-test). Thus, it was the timing of the activity relative to the reward delivery rather than the magnitude of activity induced by reward delivery that was critically involved in the microcircuit reorganization. The inter-reward interval time was 26.8 ± 3.7 s ($n=11$ sessions), which was much longer than the interval between the reward and the AR neuron activity (~2.5 s), indicating that it was unlikely that the decrease in AR neuron activity from the early to the late conditioning period occurred because these neurons had the

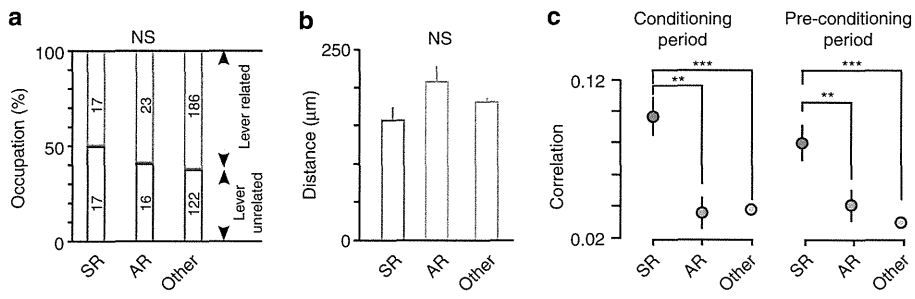

Figure 6 | Characteristics of neurons with reward-timing-dependent bidirectional modulation. (**a**) Percentage of lever-related (magenta) and lever-unrelated (blue) neurons. The number inside each bar denotes the total number of neurons. SR versus AR, $P=0.44$; AR versus other, $P=0.85$; other versus SR, $P=0.23$; χ^2-test. (**b**) Distance of SR, AR and other non-target neurons from the target neuron. SR versus AR, $P=0.084$; AR versus other, $P=0.22$; other versus SR, $P=0.26$; Wilcoxon rank sum test. (**c**) The spontaneous pairwise correlation of SR, AR and other non-target neurons with the target neuron during the conditioning period (left) and pre-conditioning period (right). Left: SR versus AR, $^{**}P<2.3\times10^{-5}$; AR versus other, $P=0.31$; other versus SR, $^{***}P=4.8\times10^{-7}$; Wilcoxon rank sum test. Right: SR versus AR, $^{**}P=0.008$; AR versus other, $P=0.53$; other versus SR, $^{***}P=1.9\times10^{-5}$; Wilcoxon rank sum test.

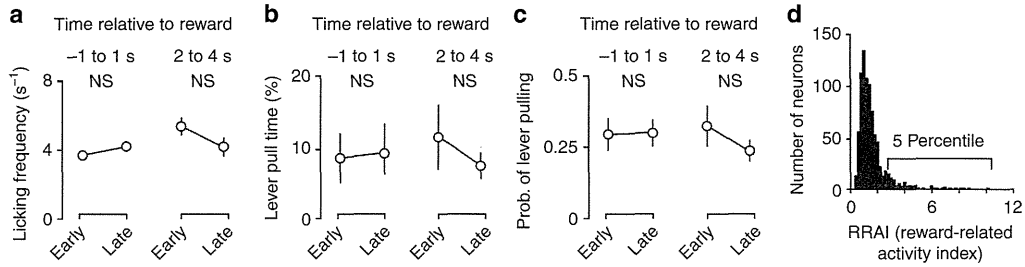

Figure 7 | Behaviours around and after reward delivery and the distribution of reward-related activity index. (**a**) Licking frequency around the time of reward delivery (-1 to 1 s) and 2 to 4 s after reward delivery in the early and late conditioning periods. −1 to 1 s, $P=0.12$, $n=11$; 2 to 4 s, $P=0.15$, $n=11$; Wilcoxon signed-rank test. (**b**) Lever-pull time around the time of reward delivery (-1 to 1 s) and 2 to 4 s after reward delivery in the early and late conditioning periods. Lever-pull time did not significantly change from the early to the late conditioning period (-1 to 1 s, $P=0.52$, $n=11$; 2 to 4 s, $P=0.52$, $n=11$; Wilcoxon signed-rank test). (**c**) The probability of lever pulling around the time of reward delivery (-1 to 1 s) and 2 to 4 s after reward delivery in the early and late conditioning periods. The probability of lever pulling did not significantly change from the early to the late period (-1 to 1 s, $P=0.73$, $n=11$; 2 to 4 s, $P=0.65$, $n=11$; Wilcoxon signed-rank test). (**d**) The histogram for reward-related activity index (RRAI) in non-target neurons in sessions with a lever-unrelated target neuron. Note that the distribution was strongly skewed. The non-target neurons with the top 5% RRAI were defined as reward-related neurons.

weakest relation to the reward of all non-target neurons. Rather, these results suggest that the activity of AR neurons decreased owing to the timing (~2.5 s) of the activity relative to reward delivery.

Pairing of ChR2 photostimulation and reward recreated RTBM. To validate whether the activity timing relative to the reward delivery is sufficient to induce the neuronal activity changes, we performed repetitive pairing of the activity of a random set of neurons and reward delivery with different time intervals. We expressed GCaMP6f[26] in a majority of the neurons and ChR2-mCherry[18] in a subset of neurons to be photostimulated (Fig. 8a; see Methods). The photostimulation was performed in mice that had not been trained to perform the lever-pull task. In each photostimulation session, 60 photostimuli were delivered during a 15 min period to induce firing in ChR2-mCherry-expressing neurons in the field of view and a reward (8 µl of water) was given 0.25 s after or 2.5 s before each photostimulation (potentiation protocol and depression protocol, respectively) (Fig. 8b). Photostimulation did not induce any observable movements. To prevent visual associative learning between the photostimulation and the reward, a blue-light-emitting diode was illuminated in front of both eyes every 2–3 s. Two-photon calcium imaging was conducted during the photostimulation period. For each reconstructed neuron,

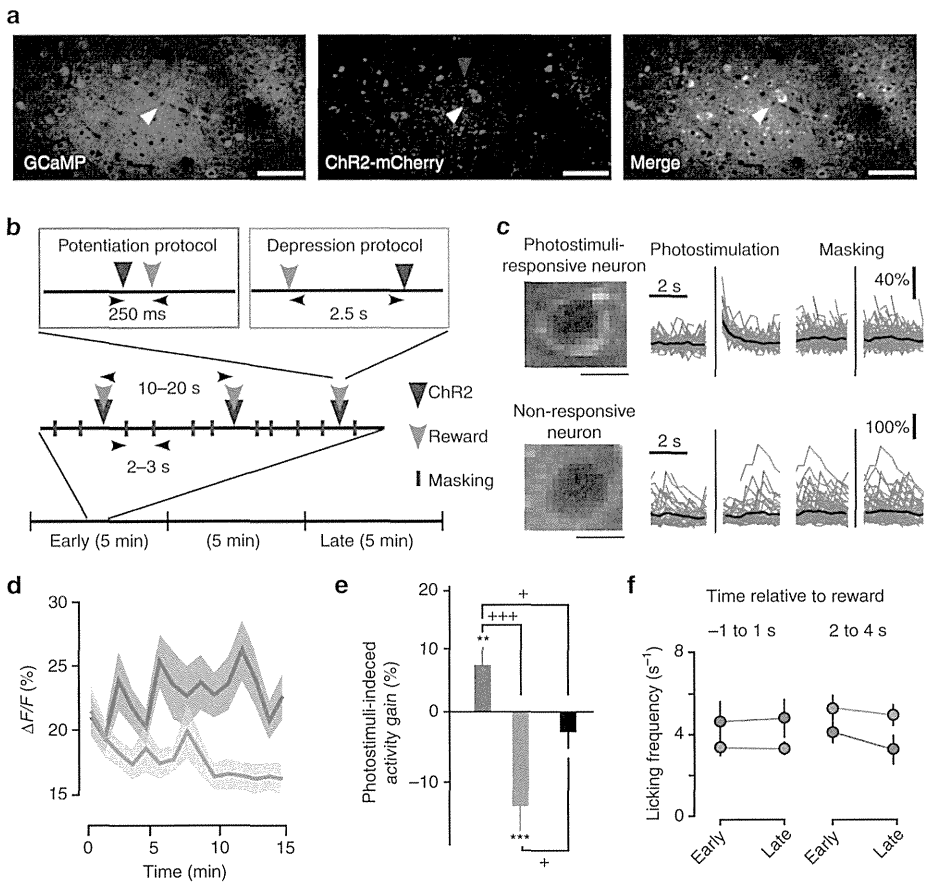

Figure 8 | Repetitive pairing of the reward and photostimulation altered the activity of photostimuli-responsive neurons. (**a**) Example images of GCaMP6f (left), ChR2-mCherry (middle) and their overlay (right) in the same field. Scale bars, 50 µm. Blue arrowheads indicate a GCaMP6f-positive and mCherry-positive neuron. White arrowheads indicate a GCaMP6f-positive and mCherry-negative neuron. (**b**) Protocols for delivering ChR2 stimuli. Blue and cyan arrowheads indicate ChR2 stimuli and reward deliveries, respectively. For masking (blue bars), a blue light was illuminated in front of the eyes every 2–3 s. (**c**) Left: Expanded images of the photostimuli-responsive neuron indicated by blue arrowheads in panel **a** (top) and the photostimuli-non-responsive neuron indicated by white arrowheads in panel **a** (bottom). Scale bars, 5 µm. Right: $\Delta F/F$ traces of these neurons aligned with ChR2 photostimulation (blue line; middle) and light masking (black line; right). The thick black traces denote the mean of all traces. Broken points in the grey traces indicate the time of unaligned masking. (**d**) Time course of the mean $\Delta F/F$ of photostimuli-responsive neurons in the potentiation (green, $n=78$ neurons) and depression (orange, $n=40$ neurons) protocols. Thick lines and shading indicate the mean ± s.e.m. (**e**) Photostimuli-induced activity gain of the photostimuli-responsive neurons in the potentiation protocol (left, green; $n=78$ in four sessions from four mice) and depression protocol (middle, orange; $n=40$ in four sessions from four mice) and 60 photostimuli without reward (right, black; $n=77$ in four sessions from three mice). Potentiation, $^{**}P=0.0081$; depression, $^{***}P=0.00040$; no-reward, $P=0.26$; one-sample t-test compared with zero. One-way analysis of variance indicated a significant difference across protocols ($P=1.8\times10^{-5}$). Crosses indicate the results of *post-hoc* pairwise comparisons: potentiation versus depression, $^{+++}P=6.1\times10^{-6}$; depression versus no-reward, $^{+}P=0.032$; no-reward versus potentiation, $^{+}P=0.019$; HSD test. (**f**) Licking frequency around the time of reward delivery (-1 to 1 s) and 2 to 4 s after reward delivery in the early and late conditioning periods. Green, potentiation protocol ($n=4$). Orange, depression protocol ($n=4$).